NTNU – Trondheim
Norwegian University of
Science and Technology

# Coping with Harmonics in Smart Grid: variable speed driveswith Back-to-Back Voltage Source Converter versus the matrix converter

Imran Ali

Master of Energy and Environmental Engineering
Submission date: July 2013
Supervisor: Marta Molinas, ELKRAFT
Co-supervisor: Nathalie Holtsmark, ELKRAFT

Norwegian University of Science and Technology
Department of Electric Power Engineering

NTNU
Norwegian University of
Science and Technology

# Coping with Harmonics in Smart Grids: Variable speed drives with the Matrix Converter versus Back-to-Back voltage source converter


**Imran Ali**


Master of Science in Energy and Environment
Submission date: July 2013
Supervisor: Marta Molinas
Co-supervisor: Nathalie Holtsmark


Norwegian University of Science and Technology
Department of Electric Power Engineering

# Description

Since the 60s the use of power electronic interfaced loads has considerably increased with the proliferation of personal computers, TV sets, adjustable speed motor drives for pumps or air conditioning appliances, etc… When these loads are connected to the grid through passive diode rectifiers, harmonics are injected into the grid. This trend has led to a harmonic pollution problem which is now subject to new regulation in the context of Smart Grids.

When using active front ends (voltage source converters) in variable speed drive systems instead of diode rectifiers it is possible to reduce the harmonic content of the grid by active filtering. By replacing some of the passive diode rectifiers with voltage source convers, the regulations on harmonic content can be met.

Similarly, the matrix converter can also be used in adjustable speed drive systems and can also provide active filtering. The matrix converter is a direct AC-AC converter that does no feature a DC link capacitor and is therefore interesting for aerospace and offshore applications where a small volume or temperature independency are important.

In the Master thesis the two drive systems with matrix converter and back-to-back voltage source converters should be compared in terms of active filtering capability. The simulation software PSIM should be used to develop models of the drive system as a first step. A simulation model of the matrix converter will be provided

And to design the LC filter for the MC converter so it avoids creating and sending the harmonics current to the grid.

## Abstract

In this master thesis it has been investigated to utilize the matrix as a shunt active power filter and an adjustable speed drive and then compare the matrix converter with the Back-to-Back voltage source converter in terms of active filtering capability and reactive power compensation.

In first steps to utilize the matrix converter as a motor drive and a shunt active power filter the control systems for the Permanent magnet synchronous machine, shunt active power filter and 3-phase LC-filter are built.

In second steps the simulation result of the matrix converter as motor drive and shunt active power filter is compared with the Back-to-Back voltage source converter in terms of active filtering.

The simulation results show that the matrix converter can operate as motor drive very well, but it cannot operate as a shunt active power filter at the same time. In other words it does not have the capability to compensate the harmonic current of the nonlinear load and to make the source current sinusoidal and harmonic free.

Whereas the simulation results for Back-to-Back voltage source converter shows that, it can operate as motor drive and a shunt active power filter at the same time. In other word Back-to-Back converter has a good capability for the harmonic current and reactive power compensation.

From the simulation results it can be concluded that the Back-to-Back voltage source converter is the best in terms of active filtering capability and reactive power compensation.

## Preface and acknowledgment

This is my Master's thesis in Electric Power Engineering which is the completion of my Master studies in Energy and Environment at the Norwegian University of Science and Technology (NTNU) in Trondheim.

I would like to thanks my research supervisors Professor Marta Molinas for providing me an interesting project. And most of all I would like to express my deep gratitude to my research co-supervisor Nathalie Holtsmark who assisted me and supervised me throughout the whole project period.

Finally, I wish to thank my friends, my sisters, brothers, and parents for their direct and indirect support and encouragement throughout my study.

Imran Ali
Trondheim, Norway
11 July 2013

Contents

# Chapter 1
# Introduction

In modern days nearly all the power from the utility to the residential, commercial and an industrial electric device are interfaced by the front-end power electronic equipment like diode and thyristor [1] [2] [3]. Such equipment is contributing to the proliferation of the harmonic current pollution. And this harmonic current pollution can cause harmonic voltage pollution. As a consequence of these harmonic current/voltage pollution, power quality in the power transmission/distribution system is deteriorated, which is a serious problem for many countries in the world [3].

To reduce the harmonic pollution and to have a “clean power” in the transmission/distribution system, the standards for the emission of the harmonic current have been introduce by IEEE 519-1992 for the USA and IEC 61000-3-2/IEC 61000-3-4 for the Europe [1].

To meet the IEE 519-1992 and IEC 61000-3-2/IEC 61000-3-4 standards, there are varieties of technique to reduce or eliminate the harmonic current/voltage; those are by application of:

I. **Passive LC-filter** [1]
II. **Harmonic cancellation by mixing of single and three phase nonlinear loads** [4]
III. **The multi-pulse rectifiers** [1]
IV. **Shunt active filters** [5]
V. **Adjustable speed drive with active filtering capability** [6]

**Passive LC-filter**

Harmonic current reduction by means of LC-filter is a classical method. Passive LC-filter can be constructed capacitor and inductor in series or parallel to the grid. “Each harmonic ($5^{th}$, $7^{th}$, $11^{th}$, $13^{th}$) require its own filter. This means that the filter cannot be designed in general way but must be designed according to each specific application” [1] see Figure 1.1.

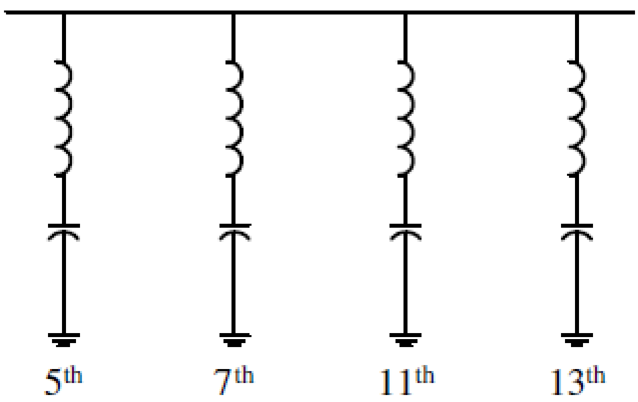


**Figure 1.1 Passive LC-filter [1]**

**Harmonic cancellation by mixing single and three phase load**

Harmonic cancellation by mixing single and three phases load is suggested in [4]. With this method the 5$^{th}$, 7$^{th}$ harmonic current of a single-phase diode rectifier are often in counter-phase with the 5th, 7$^{th}$ harmonic current of a three-phase diode rectifier, as a result it gives a reduce THD [1] [4]. See Figure 1.2 and Figure 1.3.

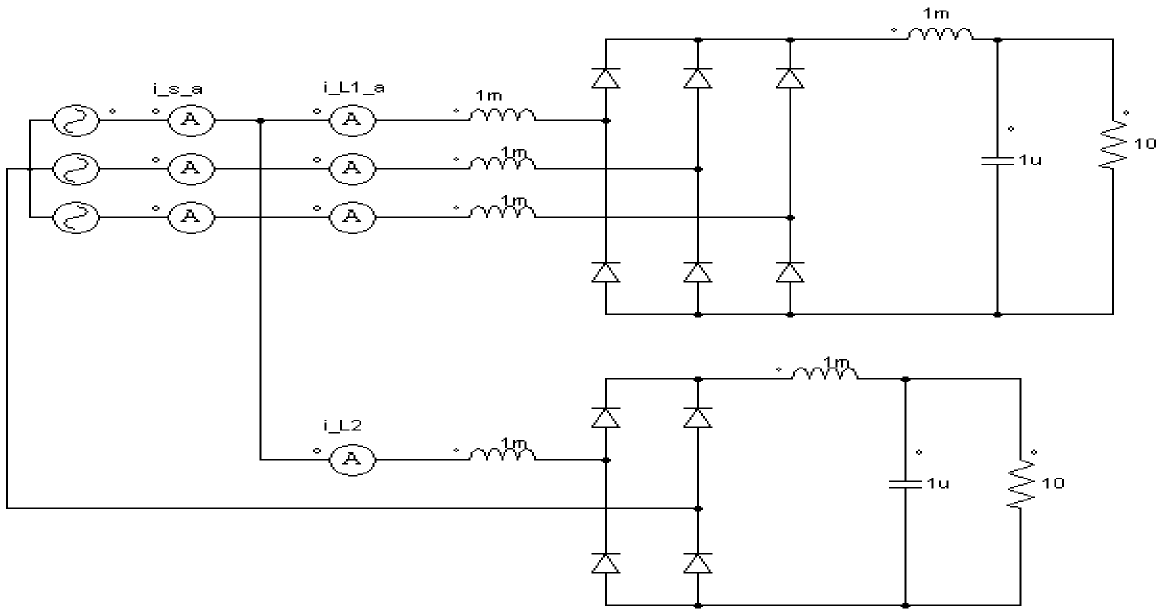


Figure 1.2 Mixing of single phase and three phases Nonlinear loads [4]

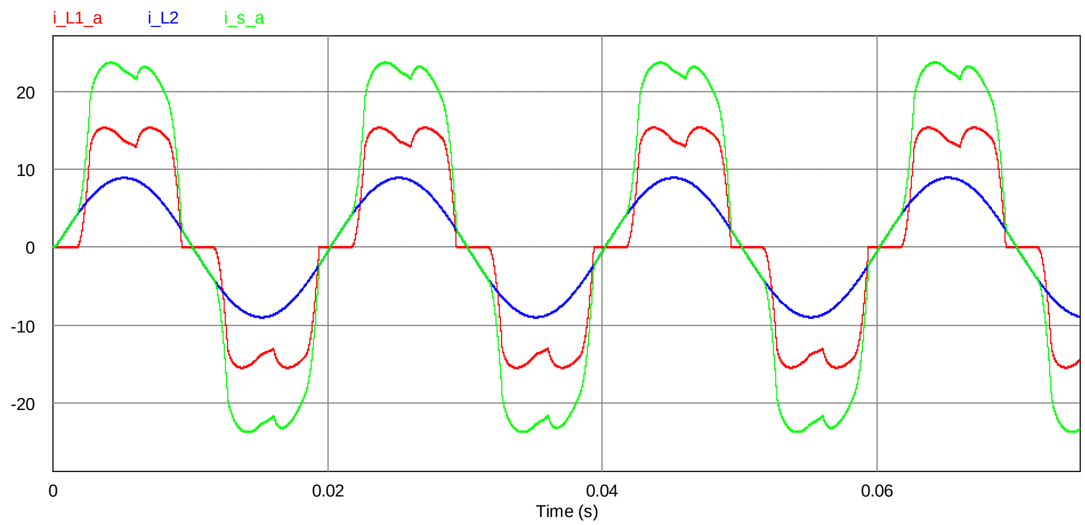


Figure 1.3 Simulation result of mixing single and three phase nonlinear loads

**The multi-pulse rectifier**

The multi-pulse rectifier technique with its simulations is presented in Figure 1.6. This method needs a bulky and heavy transformer for the cancellation and reduction of the harmonic currents. The transformer causes into higher voltage drops and higher harmonics current at non-symmetrical loads [1].

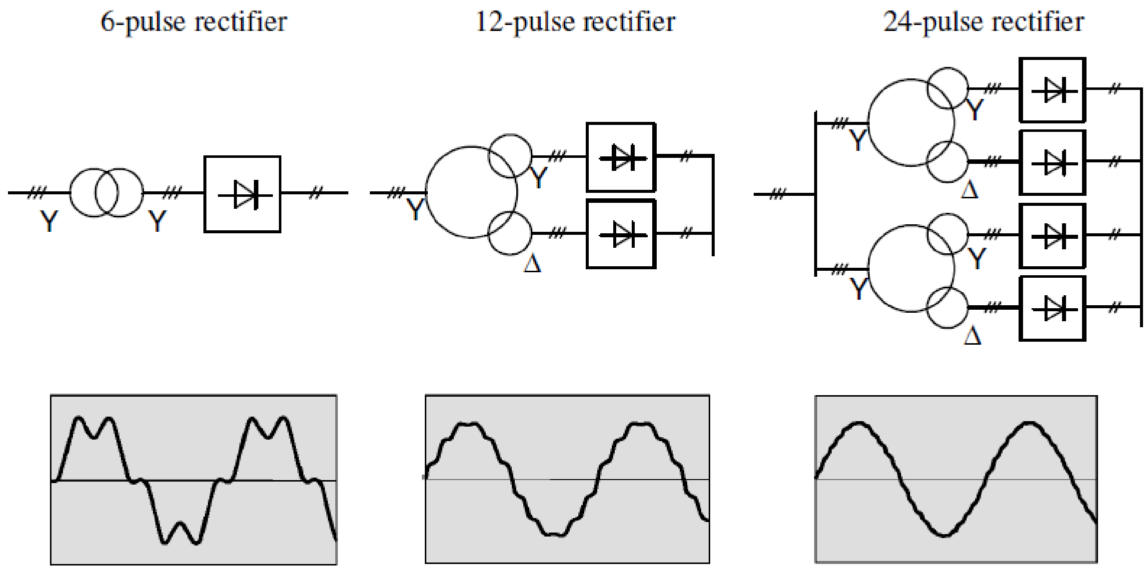


Figure 1.4 Harmonic current reduction by multi-pulse rectifier method [1]

**Shunt active filters**

Shunt active filters (SAF) is the modern filter compared to the Passive LC-filter, Mixing of single and three phase nonlinear loads and the multi-pulse rectifiers.

The shunt active filter is described in Figure 1.5 compensates/supplies the reactive and the harmonic/distortion power to the nonlinear load. Therefore the apparent power for (SAF) compensation/supply can be written as $S_{NL} = \sqrt{Q_{NL}^2 + D_{NL}^2}$. The terms $Q_{NL}$ and $D_{NL}$ is the reactive and distortion power compensations respectively.

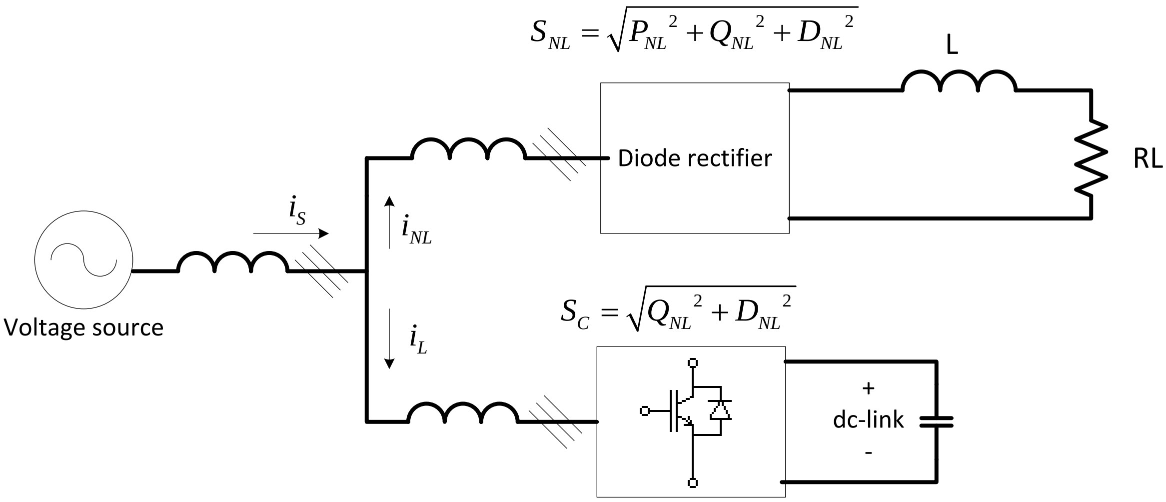


Figure 1.5 Shunt active power filter

**Back-to-Back voltage source converter as an adjustable speed drive and shunt active filter**

On the other hand the Back-to-Back (B2B) voltage source converter as an Adjustable Speed Drive (ASD) with active front end rectifier as illustrated in Figure 1.6 can also be employed as a shunt active powers filter. An ASD with active front end filter compensate/supply not only the harmonic/distortion and reactive power ($Q_{NL}$ + $D_{NL}$) to the nonlinear load, but it is also supplying Active power ($P_L$) to its own load. Hence the apparent power $S_C$ for the B2B converter with active filtering capability can be expressed as $S_C = \sqrt{P_L^2 + Q_{NL}^2 + D_{NL}^2}$.

In a conventional Back-to-Back converter as shown in Figure 1.6, the voltage source inverter and the active front end rectifier is separated by a dc-link capacitor. Previously in the specialization project "Coping with Harmonics in Smart Grids: Analysis of the Back-to-Back voltage source converter" or [7], the Back-to-Back voltage source converter has been used as shunt active power filter and an adjustable speed drive. The simulations of [7] are going to be presented in term of shunt active filtering and as adjustable speed drive in section 5.2.

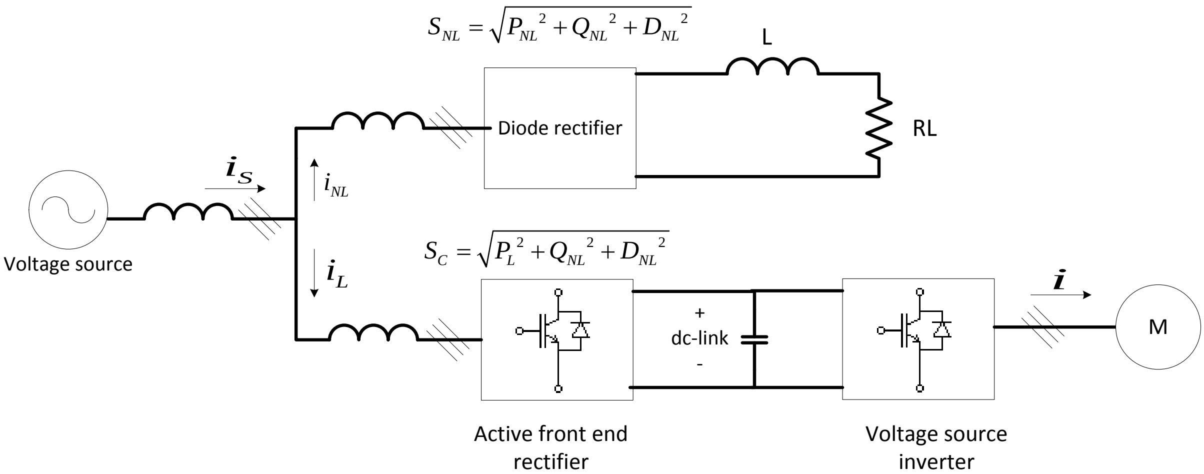


Figure 1.6 Adjustable speed drive with active filtering capability

**The matrix converter as a shunt active power filter and an adjustable speed drive**

To avoid the bulky dc-link capacitor in a conventional Back-to-Back voltage source converter, the matrix converter (MC) is under research to use it as shunt active power filter and an adjustable speed drive. Previously in reference [8] and [9] the matrix converter has been used as a shunt active power filter and also as a conversion system between the generator and the grid. It should be noted that the generator behave as active and reactive power source. Until now the matrix converter has not been used as a shunt active filter for harmonic current compensation and at the same time as an adjustable speed drive for the motor.

Therefore in this master thesis it is investigated to utilize the Matrix Converter (MC) as a shunt active filter for harmonic current compensation and a variable speed drive for the motor. The motor which is under consideration for the drive system is a Permanent Magnet Synchronous Machine (PMSM). An overview of the matrix converter which is supposed to operate as variable speed drive and a shunt active power filter is depicted in Figure 1.7.

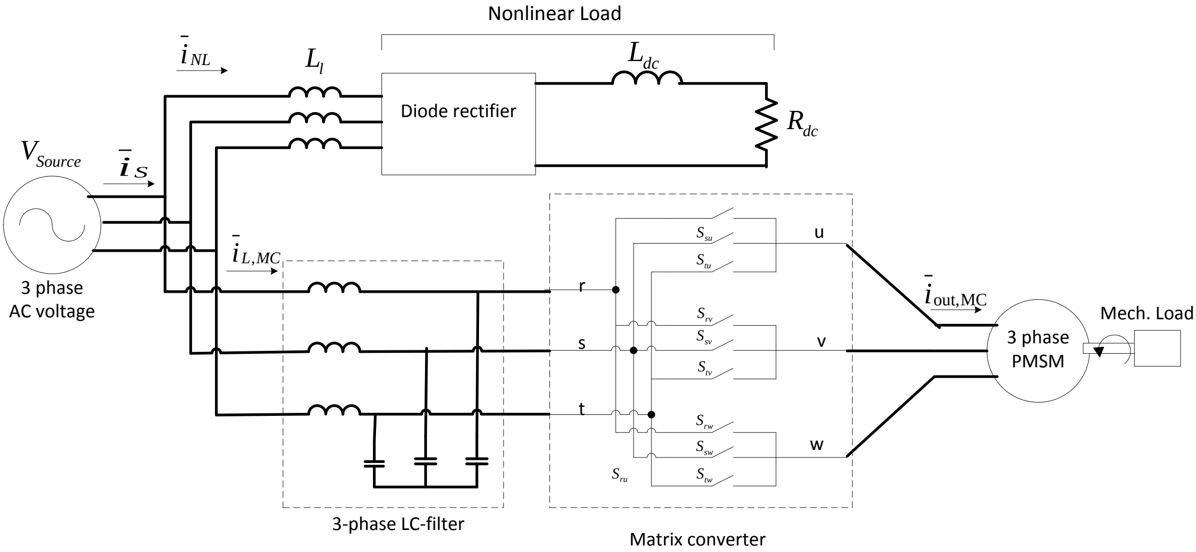


Figure 1.7 The matrix converter as an ASD and shunt active filter

In order to analyze and to check, if the matrix converter can operate as an adjustable speed drive with active filtering capability, the simulation software PSIM is used as a tool. In the simulation results part the matrix converter is going to be compared with the Back-to-Back voltage source converter [7], in terms of active filtering.

The structure of the thesis is as follows

**Chapter 1: Introduction** presents a short introduction about the harmonic pollution and its solution by different kind of the harmonic compensation technique.
**Chapter 2: The matrix converter** introduces the matrix converter and its modulation system.
**Chapter 3: The matrix converter as an adjustable speed drive:** describe how the PMSM control system is built
**Chapter 4: The matrix converter as a shunt active power filter:** describe the control method for the shunt active power filter and 3-phase LC-filter
**Chapter 5: Simulation results:** shows the simulation results of the matrix converter as an ASD and a shunt active power filter
**Chapter 6: Discussion:**
**Chapter 7: Conclusion:**

# Chapter 2
# The Matrix Converter

The Matrix converter is an AC-to-AC converter composed of nine semiconductor bidirectional switches that form a three by three matrix. These bidirectional switches are connecting each input terminal to each output terminal [10]. The matrix converter does not have energy storage component like DC-link capacitor and inductor, but it is important to have an LC-filter at the input of matrix converter [11]. The reason for having an input LC-filter is to absorb the switching harmonic of the matrix converter.

There are two types of matrix converter: Indirect matrix converter Figure 2.1 and Direct matrix converter Figure 2.2 [12].

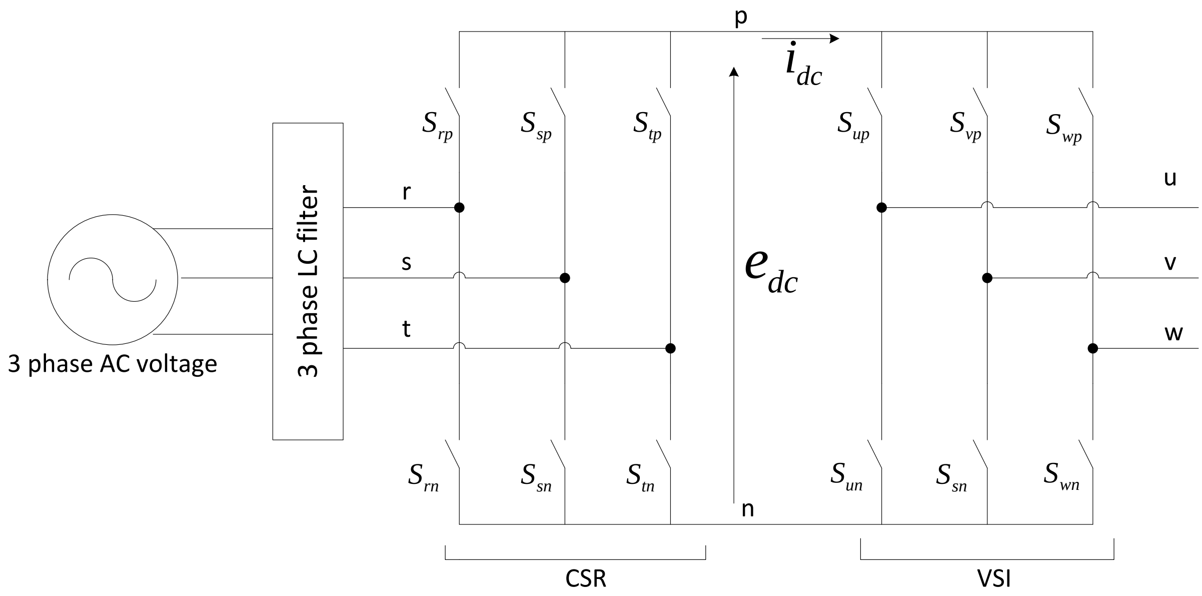


Figure 2.1 Indirect matrix converter with an input 3-phase LC-filter

An indirect matrix converter is consisting of current source rectifier (CSR) and voltage source inverter (VSI), but without energy storage component.

In the matrix converter the output voltage is limited to 0.866 of the input voltage [13]. This output voltage constrain take place due to the maximum output voltage cannot be greater than the minimum voltage differences between two phases of the input [11].

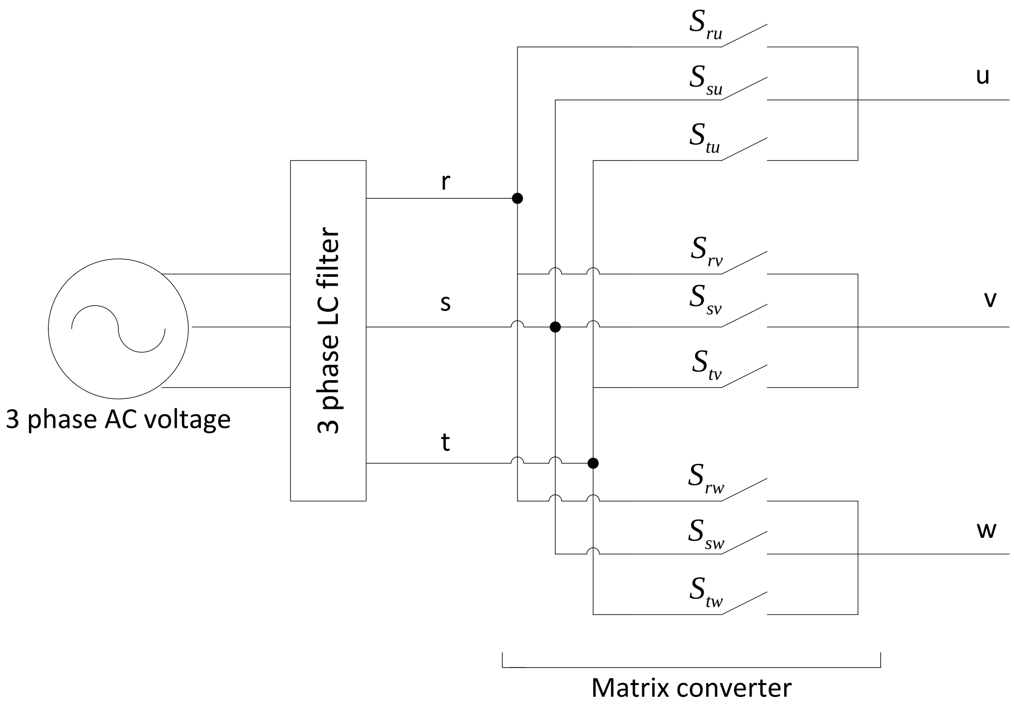


Figure 2.2 Direct matrix converter or the matrix converter with an input 3-phase LC-filter

## 2.1 Input LC filter

A three phase LC-filter is required to be connected at the input terminal of the matrix converter. The purpose of this LC-filter is to absorb and eliminate the switching harmonics of the matrix converter. The size of the input filter decreases with increasing the switching frequency of the matrix converter, which further result to switching losses [11], this can be explained by Figure 2.3.

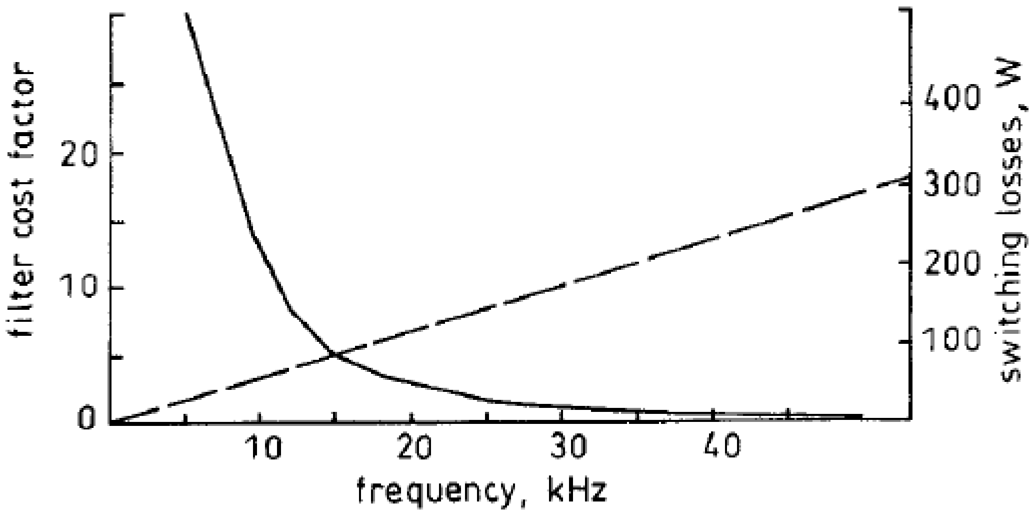


Figure 2.3 Effect of switching frequency on comparative cost of input filter [11]

This 3-phase LC-filter is prone to series and parallel resonance and harmonic both from the voltage source (grid) and the matrix converter [14].

## 2.2 Input LC filter design of the Matrix converter

The capacitor $C_f$ at the input of the matrix converter forms a LC-filter with the source impedance. Because the source inductance $L_s$ usually changes with the system operating conditions, therefore it is smart that LC filter has its own inductance $L_f$ to control the resonance frequency [14].

In reference [14] it is suggested that the total line inductance ($L_s$ + $L_f$) is normally between 0.09 - 0.15 pu, where $L_s$ is the line inductance.

For the sake of simplification in this thesis a pure 3-phase voltage source is used instead of the grid, for this reason the line inductance $L_s$ is set to be zero. Consequently it is supposed that $L_f$ is 0.05 pu, resonance frequency is 1000 Hz .The base impedance can be found as:

$$Z_{base} = \frac{V_{LL}^2}{S} \tag{2-1}$$

The line to line voltage VLL is 400 V and the apparent power is supposed to be 800 VA, as the active power of the PMSM is 785 watt. Substituting value of $V_{LL}$ and the apparent power S into equation (2-1) give the base impedance $Z_{base}$ as follow:

$$|Z_{base}| = \frac{400^2}{800} = 200\,\Omega$$

$$L_f = \frac{0.05 * |Z_{base}|}{2\pi * 50} = \frac{0.05 * 200}{2\pi * 50} = 0.03183\,H \approx 30mH$$

$$f_{res} = \frac{1}{2\pi\sqrt{L_f C_f}} \tag{2-2}$$

$$C_f = \frac{1}{(2\pi f_{res})^2 * L_f} = \frac{1}{(2\pi * 1000)^2 * 0.03183} = 7.957 * 10^{-7} \approx 1\mu F \tag{2-3}$$

## 2.3 Modulation of the matrix converter

The modulation of the matrix converter is based on a virtual indirect space vector modulation technique with a virtual Current Source Rectifier (CSR) and a virtual Voltage Source Inverter (VSI) [8]. This virtual indirect space vector modulation give 12 gating signals, six signals to the switches of (CSR) and six signals to the switches of (VSI) [9], see Figure 2.1.

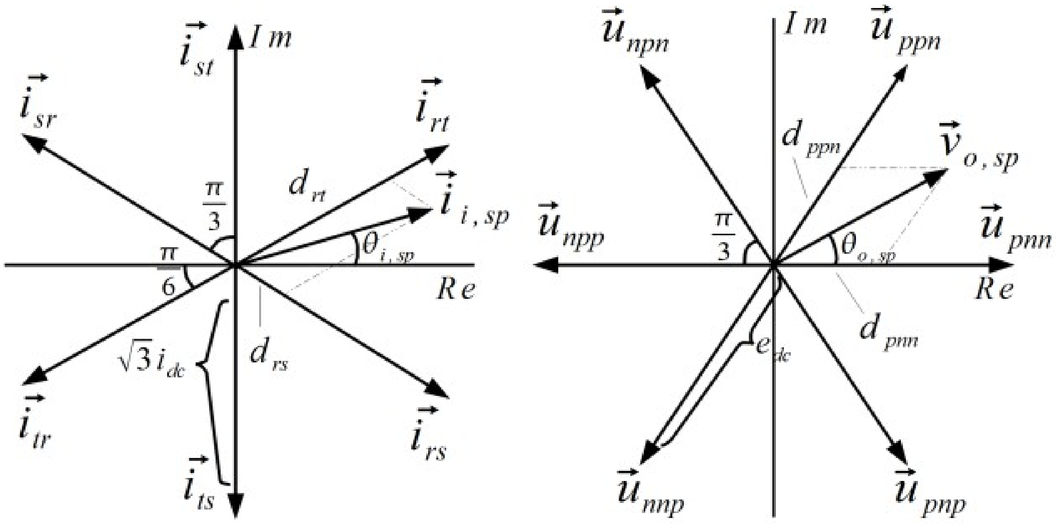


Figure 2.4 The indirect space vector modulation [9]

Using space vector modulation, the duty ratios for the VSI are calculated as follows for the first sector [9]:

$$d_{pnn} = \frac{2}{\sqrt{3}} \frac{\hat{V}_{out} \sin\left(\frac{\pi}{3} - \theta_{o,sp}\right)}{\hat{V}_{in}\, cos\emptyset} \cos\theta_{i,sp} \tag{2-4}$$

$$d_{ppn} = \frac{2}{\sqrt{3}} \frac{\hat{V}_{out} \sin\left(\theta_{o,sp}\right)}{\hat{V}_{in}\, cos\emptyset} \cos\theta_{i,sp} \tag{2-5}$$

Where $\hat{V}_{out}$ and $\hat{V}_{in}$ are the voltage amplitude of the output and an input respectively while $\emptyset$ is the input angle displacement and $\theta_{o,sp}$ is the space vectors rotational angle. At the same time the duty ratios for the CSR are calculated as follows for the first sector:

$$d_{rs} = sin\left(\frac{\pi}{3} - \left(\theta_{i,sp} + \frac{\pi}{6}\right)\right) \frac{1}{\cos\theta_{i,sp}} \tag{2-6}$$

$$d_{rt} = sin\left(\theta_{i,sp} + \frac{\pi}{6}\right) \frac{1}{\cos\theta_{i,sp}} \tag{2-7}$$

And “the duty ratios for the remaining sectors can be found by rotating the angle back to the first sector” [9].

The relationship between the input voltage and the output voltage of the matrix converter can be explained by Figure 2.2 and equation (2-8).

$$\begin{bmatrix} v_u \\ v_v \\ v_w \end{bmatrix} = \begin{bmatrix} S_{ru} & S_{su} & S_{tu} \\ S_{rv} & S_{rv} & S_{tv} \\ S_{rw} & S_{sw} & S_{tw} \end{bmatrix} \begin{bmatrix} v_r \\ v_s \\ v_t \end{bmatrix} \tag{2-8}$$

And the relationship between the input voltage and output voltage of the indirect matrix converter can be explained by Figure 2.1 and equation (2-9).

$$\begin{bmatrix} v_u \\ v_v \\ v_w \end{bmatrix} = \begin{bmatrix} S_{up} & S_{un} \\ S_{vp} & S_{vn} \\ S_{wp} & S_{wn} \end{bmatrix} \begin{bmatrix} S_{rp} & S_{sp} & S_{tp} \\ S_{rn} & S_{sn} & S_{tn} \end{bmatrix} \begin{bmatrix} v_r \\ v_s \\ v_t \end{bmatrix} \tag{2-9}$$

The 12 signals of the IMC can be converted into 9 signals for the MC, by equating equation **(2-8)** and (2-9) as:

$$\begin{bmatrix} S_{ru} & S_{su} & S_{tu} \\ S_{rv} & S_{rv} & S_{tv} \\ S_{rw} & S_{sw} & S_{tw} \end{bmatrix} = \begin{bmatrix} S_{up} & S_{un} \\ S_{vp} & S_{vn} \\ S_{wp} & S_{wn} \end{bmatrix} \begin{bmatrix} S_{rp} & S_{sp} & S_{tp} \\ S_{rn} & S_{sn} & S_{tn} \end{bmatrix} \tag{2-10}$$

$$\begin{bmatrix} S_{ru} & S_{su} & S_{tu} \\ S_{rv} & S_{rv} & S_{tv} \\ S_{rw} & S_{sw} & S_{tw} \end{bmatrix} = \begin{bmatrix} S_{up}S_{rp} + S_{un}S_{rn} & S_{up}S_{sp} + S_{un}S_{sn} & S_{up}S_{tp} + S_{un}S_{tn} \\ S_{vp}S_{rp} + S_{vn}S_{rn} & S_{vp}S_{sp} + S_{vn}S_{sn} & S_{vp}S_{tp} + S_{vn}S_{tn} \\ S_{wp}S_{rp} + S_{wn}S_{rn} & S_{wp}S_{sp} + S_{wn}S_{wn} & S_{wp}S_{tp} + S_{wn}S_{tn} \end{bmatrix} \tag{2-11}$$

From equation (2-11) it can be seen that, the 9 gate switching signals of the MC are derived from the 12 gate switching signals of IMC. And it further shows that, the relation between the input and output voltage is the same, likewise the relation between the input and output current is also the same [8].

In this project the code for indirect space vector modulation of the matrix converter is written in C++ and compiled in DLL file. This DLL file runs in parallel with PSIM and Figure 2.5 shows the physical shape of the DLL file.

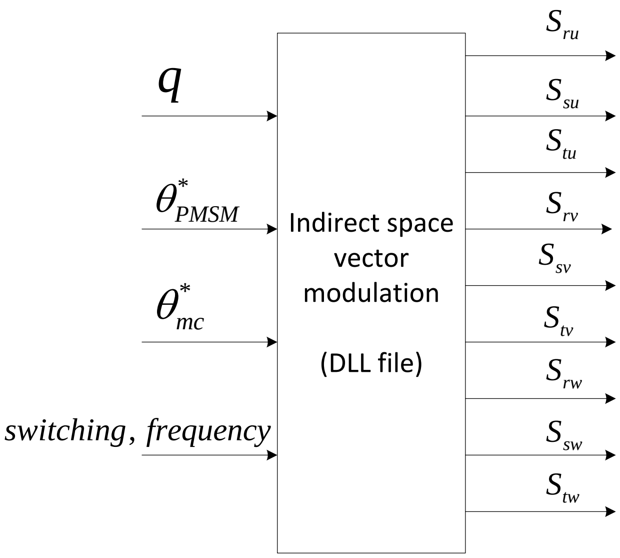


**Figure 2.5 Indirect space vector modulation**

The four inputs on the left of indirect space vector modulation (DLL file) block can be illustrated as follows

**q:** is Voltage amplitude ratio of the Voltage amplitude reference $V^*_{pms,Amp}$ to control the speed of the PMSM and the input voltage Amplitude $V_{s,Amp}$ in other word, $q = \frac{V^*_{pms,Amp}}{V_{s,Amp}}$.

$\boldsymbol{\theta^*_{PMSM}}$**:** is an angle reference from the output of the "PMSM control block", which controls the output voltage of the matrix converter and the speed of the motor.

$\boldsymbol{\theta^*_{mc}}$**:** is an angle reference from the output of "3-phase LC filter control block", which control the input current of the matrix converter and the harmonic current compensation of the nonlinear load.

The nine outputs signals on the right side of the Indirect space vector modulation block controls the on and off state of the matrix converter.

# Chapter 3
# The Matrix converter as an adjustable speed drive

In this chapter a control system of the PMSM is going to be made for the matrix converter that the matrix converter should operates as an adjustable speed drive.

## 3.1 Permanent Magnet Synchronous Motor

Here a three phase Permanent Magnet Synchronous motor (PMSM) is selected as a drive, that is due to it has a higher power density and efficiency. In addition it does not need external current source for producing rotor magnetic field as this rotor magnetic field is provided by the permanent magnet.

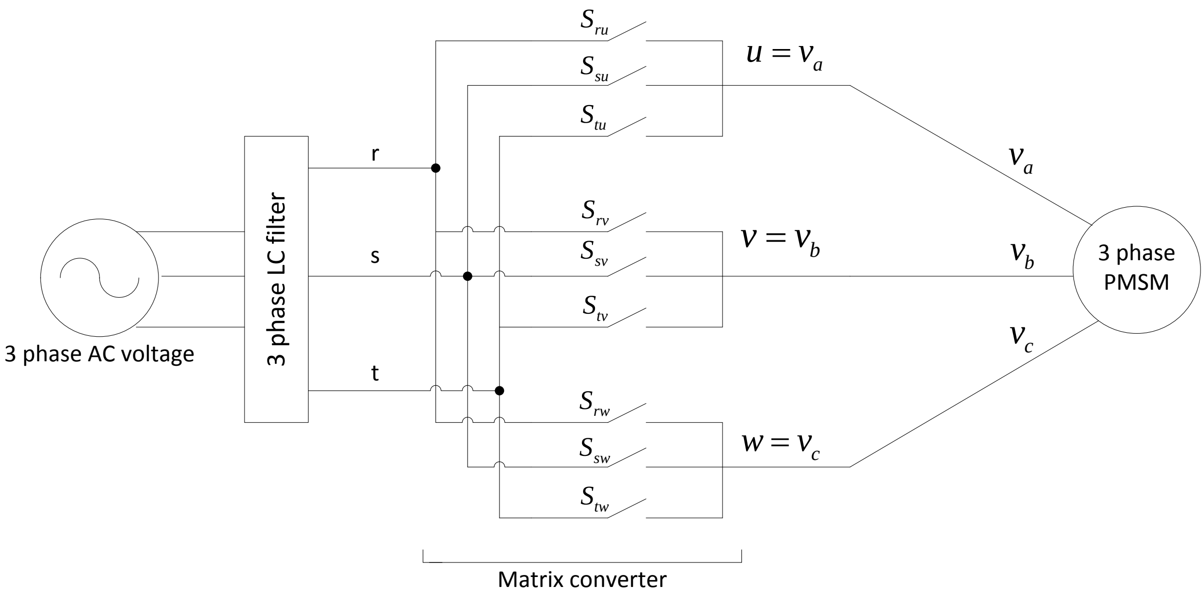


Figure 3.1 The matrix converter and 3-phase PMSM

The dynamic equivalent equation for the three phases PMSM in Figure 3.1 can be written as follows.

$$\begin{bmatrix} v_a \\ v_b \\ v_c \end{bmatrix} = \begin{bmatrix} R & 0 & 0 \\ 0 & R & 0 \\ 0 & 0 & R \end{bmatrix} \begin{bmatrix} i_a \\ i_b \\ i_c \end{bmatrix} + \frac{d}{dt} \begin{bmatrix} \lambda_a \\ \lambda_b \\ \lambda_c \end{bmatrix} \tag{3-1}$$

In equation above $i_a$ is the stator current and $\lambda_a$ is the flux linkage of phase "a". To analyze and to make the dynamic control of PMSM, equation (3-1) is transformed into dq0 coordinate system by using Parks transformation method, which is shown in equation (3-2).

$$\begin{bmatrix} v_d \\ v_q \end{bmatrix} = \begin{bmatrix} R & 0 \\ 0 & R \end{bmatrix} \begin{bmatrix} i_d \\ i_q \end{bmatrix} + \frac{d}{dt} \begin{bmatrix} \lambda_d \\ \lambda_q \end{bmatrix} + \omega \begin{bmatrix} \lambda_q \\ -\lambda_d \end{bmatrix} \tag{3-2}$$

For the sake of simplification it is assumed that the d-axis is always aligned with the rotor magnetic axis, with the q-axis 90 degree ahead in the direction of rotation, considered to be counter-clockwise [15]. Therefore the equations for the stator d- and q- winding flux linkages can be expressed as follows.

$$\lambda_d = L_d\, i_d + \lambda_{fd} \tag{3-3}$$

$$\lambda_q = L_q\, i_q \tag{3-4}$$

Where in equations (3-2) and (3-3), $L_d$ and $L_q$ is the inductance in d- and q winding respectively and $\lambda_{fd}$ is the flux linkage of the stator d-winding due to the flux produced by the rotor magnets [15]. Further to make the PMSM analysis less complex, it is presumed that the rotor of PMSM is considered to be magnetically round (non-salient) that has the same reluctance along any axis through the center of the machine, as a consequence it can be postulated as:

$$L = L_d = L_q \tag{3-5}$$

For this reason equation (3-3) and (3-4) can be presented as:

$$\lambda_d = L\, i_d + \lambda_{fd} \tag{3-6}$$

$$\lambda_q = L\, i_q \tag{3-7}$$

In equations (3-6) and (3-7) L is constant. Substituting flux linkages of equation (3-6) and (3-7) into equation (3-2), the d- and q- windings voltage can be expressed as follows, noticing that the time-derivative of the rotor-produced flux $\lambda_{fd}$ is zero [15]:

$$v_d = R\, i_d + L\frac{d}{dt} i_d + \omega\, L\, i_q \tag{3-8}$$

$$v_q = R\, i_q + L\frac{d}{dt} i_q - \omega(L\, i_d + \lambda_{fd}) \tag{3-9}$$

In balanced sinusoidal steady state the equation (3-8) and (3-9) can be simplified as follows:

$$v_d = R\, i_d + \omega\, L\, i_q \tag{3-10}$$

$$v_q = R\, i_q - \omega(L\, i_d + \lambda_{fd}) \tag{3-11}$$

Where in balanced sinusoidal steady state the term $\frac{d}{dt} i_d$ and $\frac{d}{dt} i_q$ is zero.

From equations (3-10) and (3-11) phasor equation for phase "a" in a balanced sinusoidal steady state can be written as [15]:

$$V_a = R\, I_a + j\, \omega\, L\, I_a + j\, \omega \sqrt{\frac{2}{3}}\, \lambda_{fd} \tag{3-12}$$

The equivalent circuit of the equation (3-12), under a balanced sinusoidal steady state condition is depicted in Figure 3.2.

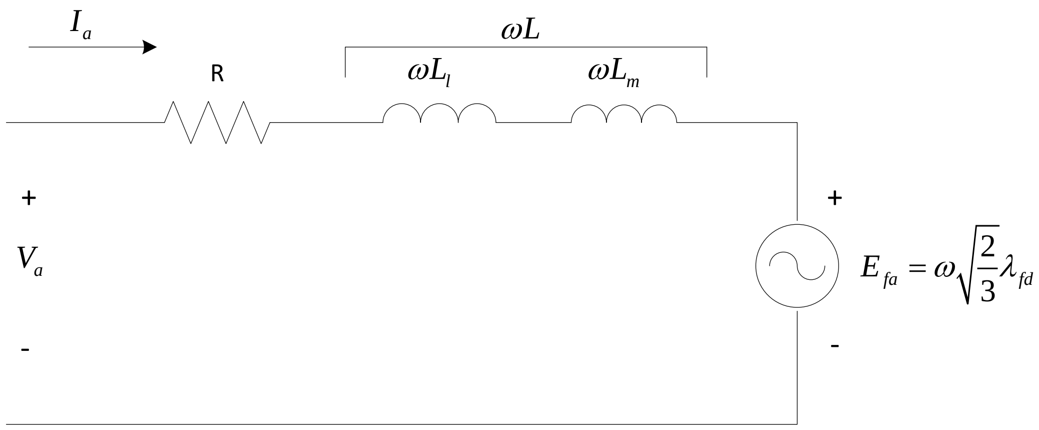


Figure 3.2 Per-Phase equivalent circuit of the PMSM in steady state

## 3.2 Electromagnetic Torque

Electromagnetic torque of the PMSM can be calculated by its apparent power at the input terminal of the PMSM.

$$S = V_s\, I_s^* \tag{3-13}$$

Where $V_s$ and $I_s$ is the stator voltage and current space vector respectively. And $I_s^*$ is the subjugate of $I_s$.

$$V_s = \sqrt{\frac{3}{2}}\,(v_d + jv_q) \tag{3-14}$$

$$I_s = \sqrt{\frac{3}{2}}(i_d + ji_q)$$

$$I_s^* = \sqrt{\frac{3}{2}}(i_d - ji_q) \tag{3-15}$$

Substituting equations (3-14) and (3-15) into equation (3-13) result into equation

$$S = \frac{3}{2}\,(v_d + jv_q)(i_d - ji_q)$$

$$S = \frac{3}{2}\{(v_d i_d + v_q i_q) - j(v_d i_q - v_q i_d)\} \tag{3-16}$$

The real part in equation (3-16) is the total active power input at the input terminal of the PMSM

$$P = \frac{3}{2}(v_d i_d + v_q i_q) \tag{3-17}$$

Substituting equations (3-8) and (3-9) into equation (3-17) results to equation (3-18)

$$P = \frac{3}{2}\left\{\left(R\, i_d + L\frac{d}{dt}i_d + \omega\, L\, i_q\right) i_d + \left(R\, i_q + L\frac{d}{dt}i_q - \,\omega(L\, i_d + \lambda_{fd})\right) i_q\right\} \tag{3-18}$$

$$P = \frac{3}{2}\left\{R\, i_d i_d + i_d L\frac{d}{dt}i_d + \omega\, L\, i_q i_d + R\, i_q i_q + i_q L\frac{d}{dt}i_q - \,\omega L\, i_d i_q - \omega\, \lambda_{fd} i_q\right\} \tag{3-19}$$

The terms $R\, i_d i_d$, $i_d L \frac{d}{dt} i_d$, $R\, i_q i_q$ and $i_q L \frac{d}{dt} i_q$ in equation (3-19) don't contribute to the output mechanical power of PMSM, so therefore these have to be ignored. As a result equation (3-19) is simplified to:

$$P = \frac{3}{2}\left\{\omega\, L\, i_q i_d - \omega L\, i_d i_q - \omega \lambda_{fd} i_q\right\}$$

$$P = -\frac{3}{2}\omega \lambda_{fd} i_q \tag{3-20}$$

Where $\omega$ is an electrical speed, in radian per second and it can be written as $\omega = \frac{p}{2}\omega_m$ ,where p is the number of poles and $\omega_m$ is the mechanical speed in radian per second. Substituting $\frac{p}{2}\omega_m$ for $\omega$ in equation (3-20), then it becomes as follows:

$$P = -\frac{3p}{4}\omega_m \lambda_{fd} i_q \tag{3-21}$$

Electromagnetic torque can be derived dividing equation above by $\omega_m$ :

$$T_{em} = \frac{P}{\omega_m} = -\frac{3p}{4}\,\lambda_{fd} i_q$$

$$T_{em} = -\frac{3p}{4}\,\lambda_{fd} i_q \tag{3-22}$$

The term on the right side in equation (3-22) is negative, this is because of the electromagnetic torque equation is derived by using the Park transformation but not a direct-quadrature-zero (or dq0) transformation. If the direct-quadrature-zero (or dq0) transformation was used for the derivation of the electromagnetic torque, then the term on the right side in equation (3-22) would have been positive. From equation (3-22) it is obvious that the electromagnetic torque is controlled by q-winding current $i_q$.

## 3.3 Electrodynamics

"The acceleration is determined by the difference of the electromagnetic torque and the load torque (including friction torque) acting on $J_{eq}$, the combined inertia of the load and the PMSM" [15]

$$\frac{d}{dt}\omega_m = \frac{T_{em} - T_L}{J_{eq}} \tag{3-23}$$

where $\omega_m$ is the mechanical speed in rad/s.

## 3.4 dq-based Dynamic Controller for PMSM Drives

To spin or to drive the PMSM by the MC at a required speed for the given mechanical load, it is important to find out its reference voltage that the MC must supply to the PMSM [15]. Writing the d-axis voltage equation of (3-8) as

$$v_d = \underbrace{R i_d + L\frac{d}{dt} i_d}_{v_d'} \quad + \underbrace{\omega\, L\, i_q}_{v_{d,comp}} \tag{3-24}$$

and the q-axis voltage equation of (3-9) as

$$v_q = \underbrace{R\, i_q + L\frac{d}{dt} i_q}_{v'_q} \;-\; \underbrace{\omega (L\, i_d + \lambda_{fd})}_{v_q, comp} \tag{3-25}$$

These two equations above make it easy to understand and to build, the d and q-axis reference voltages.

Where in equations (3-24) and (3-25)

$$v'_d = R\, i_d + L\frac{d}{dt} i_d \tag{3-26}$$

$$v'_q = R\, i_q + L\frac{d}{dt} i_q \tag{3-27}$$

And their compensation terms are

$$v_{d,comp} = \omega\, L\, i_q \tag{3-28}$$

$$v_{q,comp} = -\,\omega (L\, i_d + \lambda_{fd}) \tag{3-29}$$

The block diagram of the equations (3-23) - (3-29) is depicted in Figure 3.3.

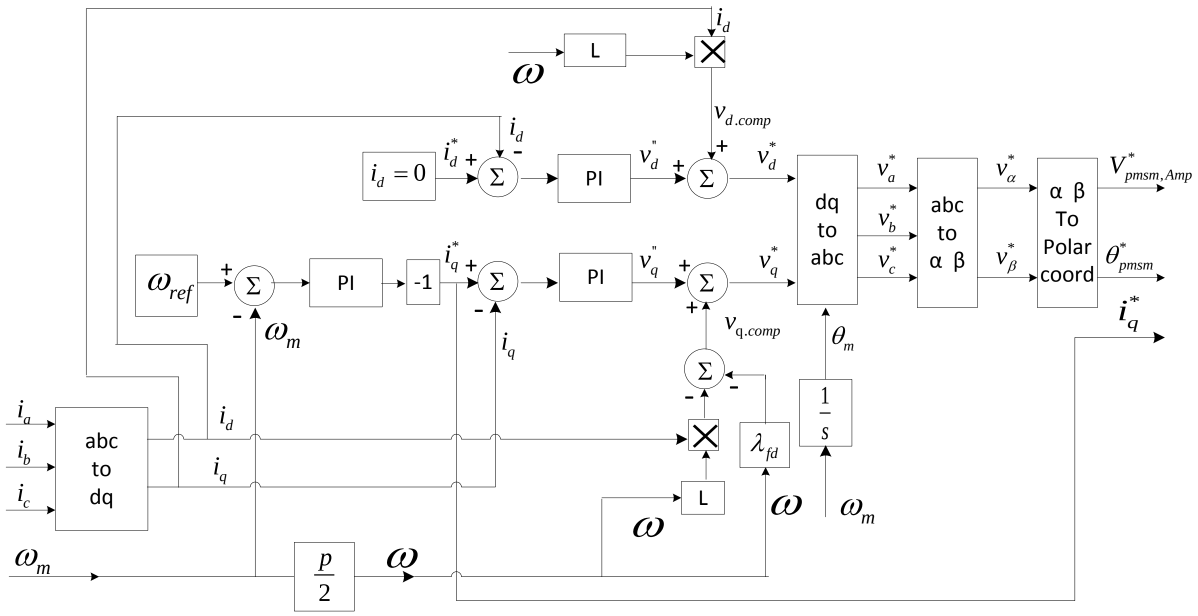


**Figure 3.3 Overview of the PMSM control**

From Figure 3.3 it is obvious that the reference value $v_d^*$ is the sum of the terms $v'_d$ and the compensation terms $v_{d,comp}$ and the reference value $v_q^*$ is the sum of the term $v'_q$ and the compensation term $v_{q,comp}$. While the values $v'_d$ and $v'_q$ are generated by the current (inner) and speed (outer) control loops.

## 3.5 Designing the PMSM

The PMSM used here is designed for a rated power of 785 watt, rated mechanical speed $\omega_{ref}$ of 157 rad/s and a rated torque of 5 Nm. The parameter of the PMSM is as follows:

| Parameter of the PMSM | | | | | | |
|---|---|---|---|---|---|---|
| $L = L_d = L_q$ | R | Vpk/krpm | p | $J_{eq}$ | tau | $\lambda_{fd}$ |
| 0.05 H | 0.05 Ω | 200 V/krpm | 4 | 0.00179 $kgm^2$ | 10s | 0.852 weber |

$V_{pk}$/krmp is the peak line-to-line back emf constant; in V/krpm for the mechanical speed of 1000 rpm.

Whereas $\lambda_{fd}$ is a magnetizing flux which can be calculated for the rated electrical speed of 314 rad/s and peak line-to-line back emf of 200 V/krpm:

$$\lambda_{fd} = \frac{V_{pk}}{\frac{p}{2}\omega_m} = \frac{200}{\frac{4}{2} * 157} = 0.6369\ weber \qquad (3\text{-}30)$$

## 3.6 Designing the PI Controller for the speed-control (outer) loop

The q-winding current reference $i_q^*$ is obtained by using a PI controller for the speed control loop, which is depicted in Figure 3.4. To avoid flux weakening and to simplify the control system, it is supposed that the mechanical speed $\omega_m$ do not exceed the rated mechanical speed $\omega_{ref}$. Therefor the reference for the d-winding current $i_d^*$ is kept zero ($i_d^*$ = 0) [15], this is also shown in Figure 3.2.

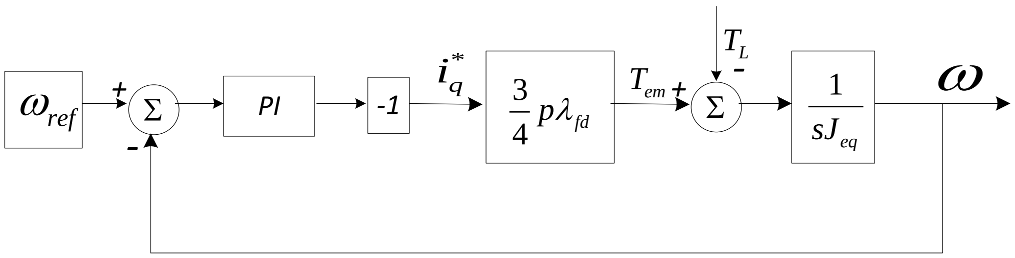


Figure 3.4 Speed-control (outer) loop

For the sake of simplification, the torque disturbance and the gain -1 due to Park's transformation are removed from the speed control loop in Figure 3.4, which results into Figure 3.5.

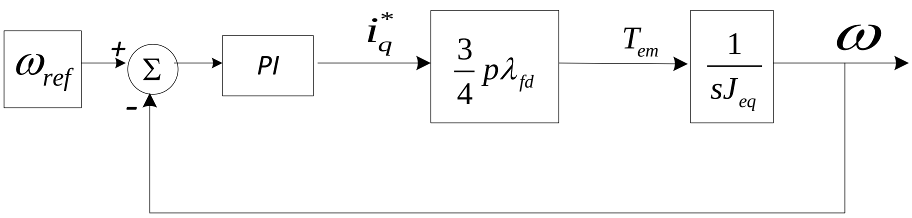


Figure 3.5 Simplified form of speed-control (outer) loop

Where the transfer function of the PI controller is defined as:

$$G(s) = k\frac{1 + Ts}{Ts} \qquad (3\text{-}31)$$

The gain k and the time constant T of the PI controllers can be found by taking the transfer function of the speed-loop in Figure 3.5.

$$H(s) = \frac{\omega_m}{\omega_{ref}} = \frac{3kp\lambda_{fd}}{4TJ_{eq}} \left( \frac{1+Ts}{s^2 + \frac{3kp\lambda_{fd}}{4J_{eq}} s + \frac{3kp\lambda_{fd}}{4TJ_{eq}}} \right) \tag{3-32}$$

$$H(s) = \omega_0^2 \left( \frac{1+Ts}{s^2 + 2\xi\omega_0 s + \omega_0^2} \right) \tag{3-33}$$

The bandwidth $\omega_0$ of the speed-control (outer) loop is chosen $\omega_0 = 62.8$ rad/s and the damping coefficient $\xi$ = 0.7071

The gain of the PI controller for the speed control loop is calculated as follows [16] [17]:

$$2\xi\omega_0 = \frac{3kp\lambda_{fd}}{4J_{eq}}$$

$$k = \frac{8\xi\omega_0 J_{eq}}{3p\lambda_{fd}} = \frac{8 * 0.7071 * 62.8 * 0.00179}{3 * 4 * 0.852} = 0.0622 \tag{3-34}$$

And the time constant T of the PI controller for the speed control loop is calculated as follows [16] [17]:

$$\omega_0^2 = \frac{3kp\lambda_{fd}}{4TJ_{eq}}$$

$$T = \frac{3kp\lambda_{fd}}{4J_{eq}\omega_0^2} \tag{3-35}$$

$$T = \frac{3p\lambda_{fd}}{4J_{eq}\omega_0^2} \frac{8\xi\omega_0 J_{eq}}{3p\lambda_{fd}} = \frac{2\xi}{\omega_0} \tag{3-36}$$

$$T = \frac{2\xi}{\omega_0} = \frac{2 * 0.7071}{62.8} = 0.0225 \tag{3-37}$$

## 3.7 Designing the PI Controllers for the current-control (inner) loop

The signals $v_d'$ and $v_q'$ in Figure 3.2, are obtained by using PI controllers in the current-control loops [15], this current-control-loop for q-axis (same for d-axis) is depicted in Figure 3.6.

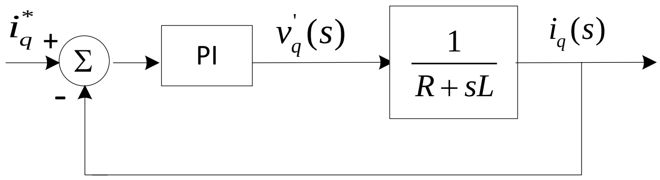


Figure 3.6 Current-control (inner) loop

The system or "motor-load plant" in the current-control-loop of Figure 3.6 is represented by the transfer function below, based on equations (3-26) and (3-27):

$$i_d(s) = \frac{1}{R + Ls} v'_d(s) \tag{3-38}$$

$$i_q(s) = \frac{1}{R + Ls} v'_q(s) \tag{3-39}$$

The gain k and the time constant T of the PI controllers can be found by taking the transfer function of the current control loop of the Figure 3.6.

$$H(s) = \frac{i_q}{i_q^*} = \frac{k\frac{1+Ts}{Ts}\left(\frac{1}{R+Ls}\right)}{1 + k\frac{1+Ts}{Ts}\left(\frac{1}{R+Ls}\right)} \tag{3-40}$$

$$H(s) = \frac{k(1+Ts)}{Ts(R+Ls) + k(1+Ts)} \tag{3-41}$$

$$H(s) = \frac{k}{TL}\left(\frac{1+Ts}{s^2 + \frac{R+k}{L}\, s + \frac{k}{TL}}\right) \tag{3-42}$$

the transfer function in equation (3-42) is of second order with one zero, which can also be written in the form of equation (3-43).

$$H(s) = \omega_0^2 \left(\frac{1+Ts}{s^2 + 2\xi\omega_0\, s + \omega_0^2}\right) \tag{3-43}$$

In equation (3-43) the term $\omega_0$ is the bandwidth of the current control (inner) loop, this bandwidth for the current control loop is selected to be $\omega_0 = 2\pi 100 = 628.32$, and $\xi$ is the damping coefficient, which is selected to be 0.7071.

The gain of the PI controller for the current control loop is calculated as follows [16] [17]:

$$\begin{gathered} 2\xi\omega_0 = \frac{R+k}{L} \\ k = 2\xi\omega_0 L - R = 2 * 0.7071 * 628.32 * 0.05 - 0.05 = 44.38 \end{gathered} \tag{3-44}$$

And the time constant of the PI controller for the current control loop is calculated as follow:

$$\begin{gathered} \omega_0^2 = \frac{K}{TL} \\ T = \frac{k}{\omega_0^2 L} = \frac{44.38}{628.32^2 * 0.05} = 0.0022 \end{gathered} \tag{3-45}$$

Once the reference voltages $v_d^*$ and $v_q^*$ are obtained, then these are transformed from dq coordinate to the abc coordinate based on the mechanical angle $\theta_m$ , from abc to alpha-beta coordinate and from alpha-beta to polar coordinate, as illustrated in Figure 3.3.

# Chapter 4
# The Matrix converter as a shunt Active power filter

It is expected that the matrix converter should also operates as a shunt Active power filter beside as an adjustable speed drive. In other words this can be described as, when the matrix converter is operating as a shunt active power filter it has to compensate/supplies the reactive power $Q_{NL}$ and the distortion power $D_{NL}$ to the nonlinear load. At the same time when the matrix converter is operating as an adjustable speed drive, it has to supply a controllable active power $P_L$ from the source to the PMSM. See Figure 4.1 for further illustration. Mathematically the apparent power for the matrix converter operating as a shunt active power filter and an adjustable speed drive can be written as $S = \sqrt{P_L^2 + Q_{NL}^2 + D_{NL}^2}$ .

Therefore in this chapter the control strategy of the harmonic current injection, reactive power compensation from the matrix converter to the nonlinear load and an active power $P_L$ supply from the source to the PMSM by the matrix converter are going to be discussed.

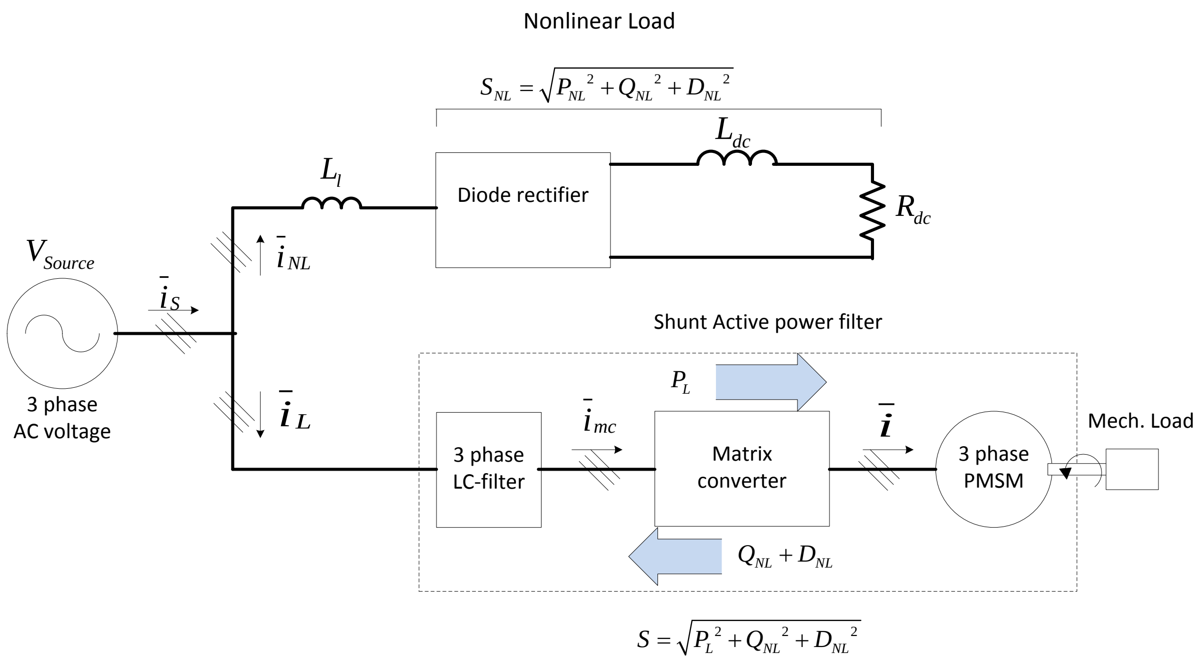


**Figure 4.1 Overview of the matrix converter as a shunt active power filter and an adjustable speed drive**

## 4.1 Shunt active power filter control and 3-phase LC-filter control

A shunt Active Power Filter (SAPF) is power converters that detects the harmonic spectrum of the non-linear load current " $\bar{\imath}_{NL}$ " and generate/inject the current " $\bar{\imath}_L$ " , which ideally is of the same harmonic spectrum as the non-linear load current but of the opposite phase. As a consequence it makes the source current " $\bar{\imath}_S$ " sinusoidal in Figure 4.1.

The objective of the Shunt Active Filter control is to detect the harmonic spectrum of the non-linear load current " $\bar{\imath}_{NL}$" and then compensates this with " $\bar{\imath}_L$" . And the purpose of the 3-phase LC-filters control is to eliminate the resonance in the LC-filter.

Figure 4.2 shows a per-phase equivalent circuit of the system under consideration. The notation $\bar{x}$ indicates a vector containing the three phases “abc”.

The control strategy of the SAPF and a 3-phase LC-filter control is consist of two cascaded control loops, those are:

1 Current-control (outer) loop
2 Voltage-control (inner) loop

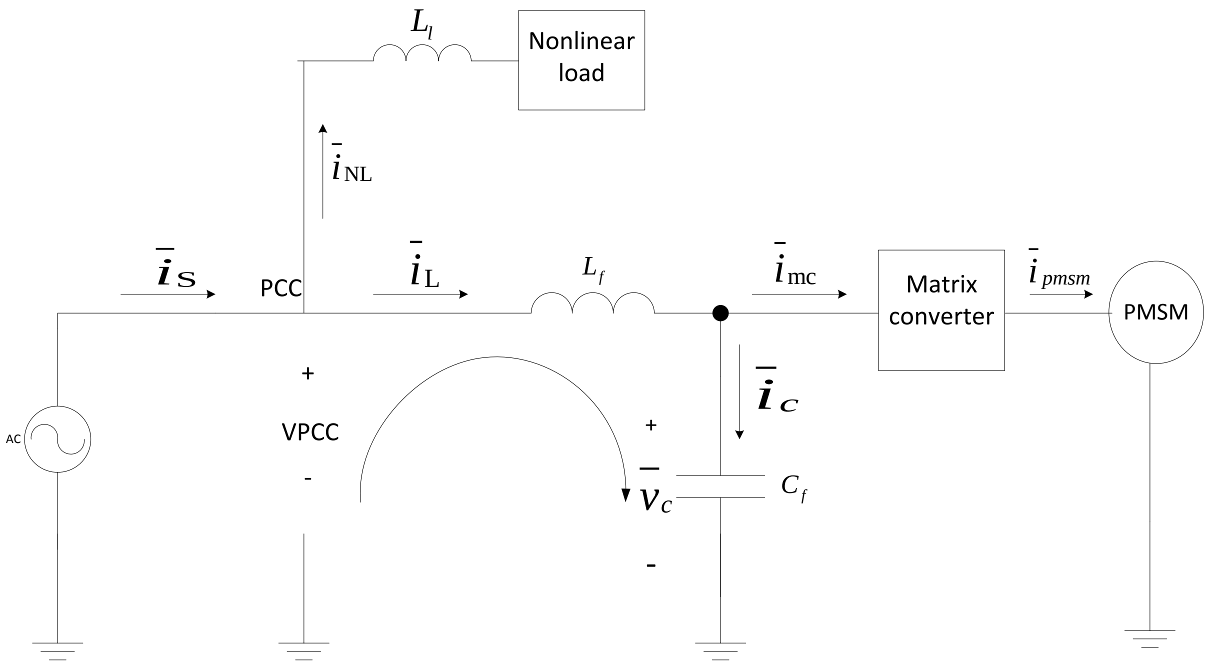


Figure 4.2 Per-phase equivalents circuit of the matrix converter and nonlinear load

Before starting to build the current control loop, it is necessary to have a prepared current reference for the current controller. The next sections explain how to build the current reference.

### 4.1.1 Current reference for the current-control loop

To obtain the current reference of the current control loop, the nonlinear-load current is measured and transformed from the fixed abc-reference frame to the rotating dq-reference frame, based on the voltage angle reference $\theta_{pcc}$ at the Point of Common Coupling (PCC), this can also be explained by the equation (4-1) and Figure 4.3.

$$\begin{bmatrix} i_{NL,d} \\ i_{NL,q} \end{bmatrix} = \frac{2}{3}\begin{bmatrix} \cos(\theta_{pcc}) & \cos\left(\theta_{pcc}-\frac{2\pi}{3}\right) & \cos\left(\theta_{pcc}+\frac{2\pi}{3}\right) \\ \sin(\theta_{pcc}) & \sin\left(\theta_{pcc}-\frac{2\pi}{3}\right) & \sin\left(\theta_{pcc}+\frac{2\pi}{3}\right) \end{bmatrix}\begin{bmatrix} i_{NL,a} \\ i_{NL,b} \\ i_{NL,c} \end{bmatrix} \tag{4-1}$$

In equation (4-1) $i_{NL,d}$ is an active current of the nonlinear-load while $i_{NL,q}$ is a reactive current of the nonlinear-load. The control intention of the Shunt Active Power filter is to compensate all the nonlinear-load's current and the reactive current $i_{NL,q}$ except for the fundamental active load current component [9] [8]. Therefore in Figure 4.3 a High Pass Filter (HPF) is proposed to filter out the fundamental component of the active current.

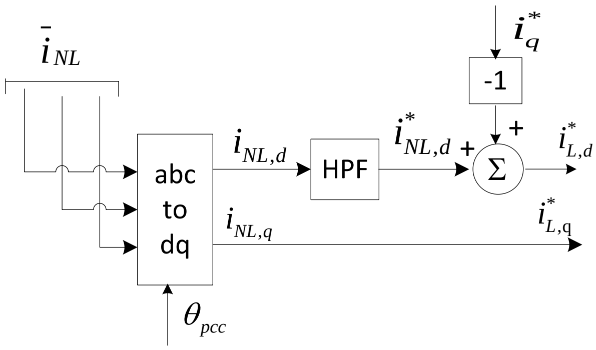


**Figure 4.3 Block diagram for reference current calculation [9]**

The q-axis current reference $i_q^*$ obtained from section 3.6 in Figure 3.3 is an active current, which control the electromagnetic torque and the active power of the PMSM. Therefore in Figure 4.3 this current is multiplied with the gain (-1) in and then added to $i_{NL,d}^*$ to obtain the active current reference $i_{L,d}^*$ , while the reactive current reference $i_{L,q}^*$ is the same as $i_{NL,q}$ in other word $i_{L,q}^* = i_{NL,q}$. These $i_{L,d}^*$ and $i_{L,q}^*$ is the active and the reactive current reference for the current control loop which is discussed in next section.

### 4.1.2 Current-control (outer) loop

Having the current reference from the previous section, now the inductor current or the current injection $\bar{\imath}_L$ into the PCC in Figure 4.2 can be controlled according to reference current. This current control loops makes the capacitor voltage reference $v_{c,d}^*$ and $v_{c,d}^*$ for the inner loop as depicted in Figure 4.4. To control the current, Kirchhoff's voltage law is applied in Figure 4.2, in order to obtain the dynamic equation (4.2) for the current $\bar{\imath}_L$.

$$L_f \frac{d}{dt}\begin{bmatrix} i_{L,a} \\ i_{L,b} \\ i_{L,c} \end{bmatrix} = \begin{bmatrix} v_{pcc,a} \\ v_{pcc,b} \\ v_{pcc,a} \end{bmatrix} - \begin{bmatrix} v_{c,a} \\ v_{c,b} \\ v_{c,c} \end{bmatrix} \tag{4.2}$$

Transforming equation (4.5), into the rotating dq coordinate system based on the voltage angle reference $\theta_{pcc}$ at the Point of Common Coupling, results into the equation

$$L_f \frac{d}{dt}\begin{bmatrix} i_{L,d} \\ i_{L,q} \end{bmatrix} = \begin{bmatrix} V_{pcc,d} \\ 0 \end{bmatrix} - \begin{bmatrix} V_{c,d} \\ V_{c,q} \end{bmatrix} + L_f\omega \begin{bmatrix} -i_{L,q} \\ i_{L,d} \end{bmatrix} \tag{4-3}$$

The phrase $L_f\omega \begin{bmatrix} -i_q \\ i_d \end{bmatrix}$ and $\begin{bmatrix} V_{pcc,d} \\ 0 \end{bmatrix}$ in equation above are cross-coupling term, and the block diagram for equation (4-3) is depicted in Figure 4.4.

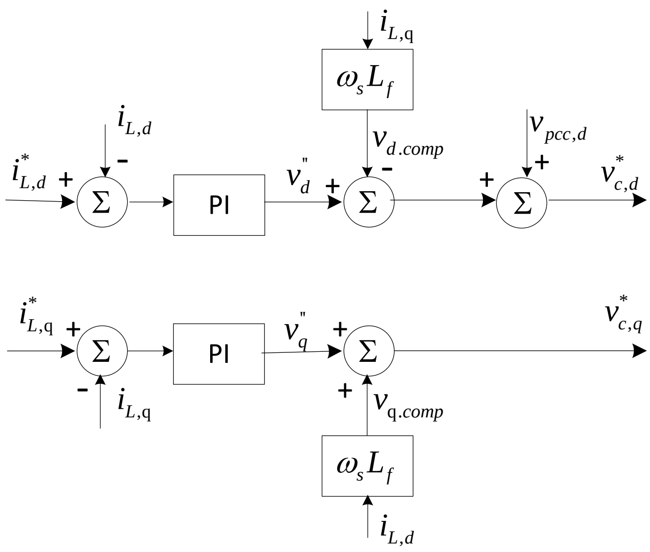


Figure 4.4 Block diagram of current-control

### 4.1.3 Designing the PI controller for the current-control (outer) loop

The gain $k_L$ and the time constant $T_L$ of the PI controller for the current control loop can be found by simplifying equation (4-3) into equation (4-4), that is by neglecting the cross coupling terms $L_f \omega \begin{bmatrix} -i_q \\ i_d \end{bmatrix}$ and $\begin{bmatrix} V_{pcc,d} \\ 0 \end{bmatrix}$.

$$L_f \frac{d}{dt} \begin{bmatrix} i_d \\ i_q \end{bmatrix} = - \begin{bmatrix} V_{cd} \\ V_{cq} \end{bmatrix} \tag{4-4}$$

By taking the transfer function of the d-coordinate in equation **(4-4)** results to:

$$L_f \, s \, i_d = -v_{cd} \tag{4-5}$$

$$H(s) = \frac{i_d}{v_{cd}} = -\frac{1}{L_f s} \tag{4-6}$$

The current control loop and equation (4-6) can be defined in the form of Figure 4.5.

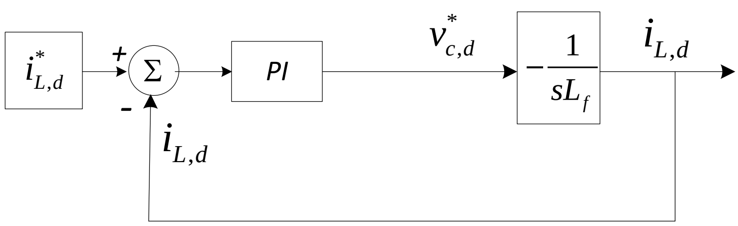


Figure 4.5 Current-control (outer) loop

Where $PI = k_L \frac{1+T_L s}{T_L s}$ and the transfer function of the current control loop in Figure 4.5 can be expressed as

$$H(s) = \frac{i_{L,d}}{i_{L,d}^*} = -\frac{k_L}{T_L L_f}\left(\frac{1 + T_L s}{s^2 - \frac{k_L}{L_f}s - \frac{k_L}{TL_f}}\right) \tag{4-7}$$

Selecting the bandwidth $\omega_{0,L}$ equal to 628.318 rad/s, the gain $k_L$ and the time constant $T_L$ of the PI controller can be found as [16] [17]

$$2\xi\omega_{0,L} = -\frac{k_L}{L_f}$$

$$k_L = -2\xi\omega_{0,L}L_f = -2 * 0.7071 * 628.318 * 0.03 = -26.65$$

$$T_L = \frac{2\xi}{\omega_{0,L}} = 2 * \frac{0.7071}{628.318} = 0.00225$$

The gain $k_L$ and time constant $T_L$ for the q-coordinate of the current control loop is the same as the d-coordinate of the current control loop.

Simulating for the gain $k_L = -26.65$ and time constant $T_L = 0.00225$, the d- and q-coordinate voltage reference $v_d^*$ and $v_q^*$ for the inner control loop is depicted in Figure 4.6.

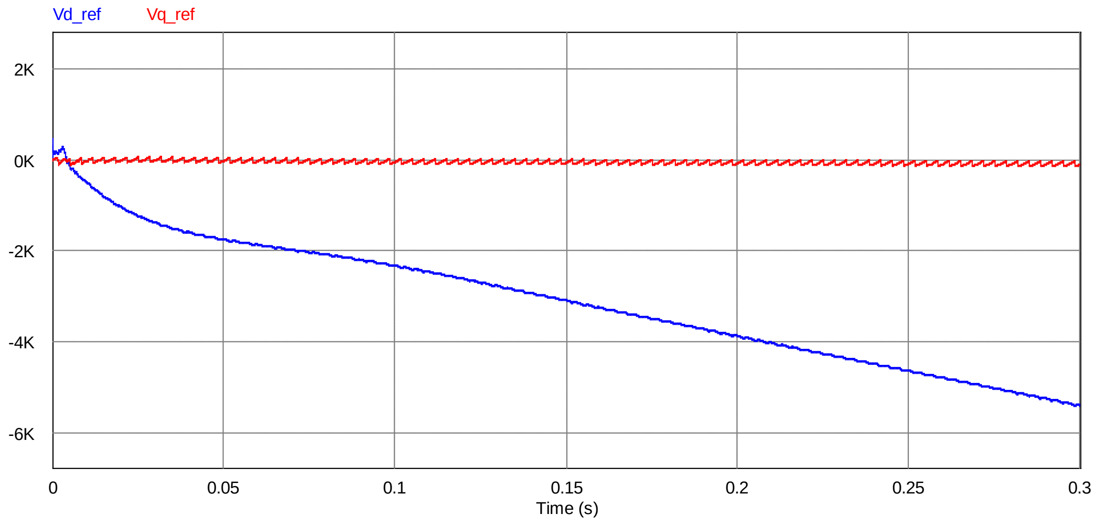


**Figure 4.6 Simulation result of voltage reference $v_d^*$ and $v_q^*$ for the gain $k_L$ = -26.65 and time constant $T_L$ =0.00225**

Figure 4.6 shows that the q- and d-coordinate voltage reference (vq_ref =$v_q^*$) in red and (vd_ref = $v_d^*$) in blue respectively. The q-coordinate voltage reference (vq_ref =$v_q^*$) is constant and stable but the d-coordinate voltage reference (vd_ref = $v_d^*$) goes to minus infinity (-∞) with the time, which cause the instability in the control system. This means that the gain $k_L = -26.65$ and time constant $T_L = 0.00225$ are not the optimum values.

After many simulations by trial and error the optimum and suitable gain $k_L$ and time constant $T_L$ for the PI controller of the current control loop both for d- and q-coordinate are found to be -0.5 and 0.045 respectively. This assertion can be proved by the simulation result in Figure 4.7.

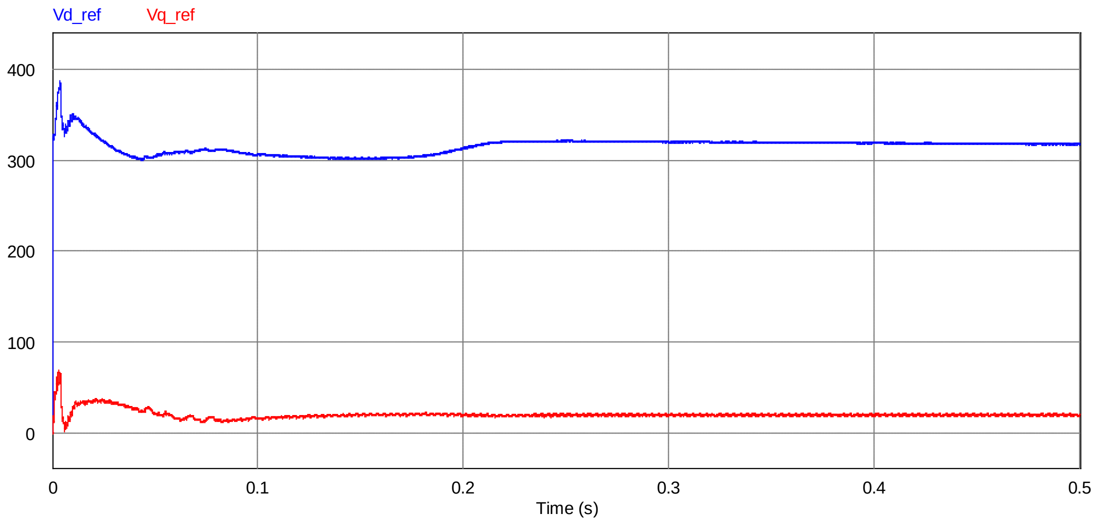


**Figure 4.7 Simulation result of voltage reference $v_d^*$ and $v_q^*$ for the gain $k_L$ = -0.5 and time constant $T_L$ =0.045**

In Figure 4.7 it can be seen that the d- and q-coordinate voltage reference, which are (vd_ref = $v_d^*$) in blue and (vq_ref =$v_q^*$) in red are stable.

The addition of the cross-coupling terms $L_f\omega\begin{bmatrix}-i_q\\ i_d\end{bmatrix}$ and $\begin{bmatrix}V_{pcc,d}\\ 0\end{bmatrix}$ to the output of PI controller in current-control loops make the voltage reference $v_{c,d}^*$ and $v_{c,d}^*$ for the capacitor voltage control (inner) loop as depicted in Figure 4.4.

## 4.2 Voltage-control (inner) loop

Likewise to control the capacitor voltage $\bar{v}_c$ and to provide the current reference $\bar{\iota}_{mc}$ to the matrix converter, the dynamic equation **(4-8)** for the capacitor voltage can be obtain from Figure 4.2

$$\begin{bmatrix} i_{L,a} \\ i_{L,b} \\ i_{L,c} \end{bmatrix} = C_f \frac{d}{dt} \begin{bmatrix} v_{c,a} \\ v_{c,b} \\ v_{c,c} \end{bmatrix} + \begin{bmatrix} i_{mc,a} \\ i_{mc,b} \\ i_{mc,c} \end{bmatrix} \quad (4\text{-}8)$$

Transforming equation (4-8) into the rotating dq coordinate system based on the voltage angle reference $\theta_{pcc}$ at the Point of Common Coupling, result to equation below:

$$\begin{bmatrix} i_{L,d} \\ i_{L,q} \end{bmatrix} = C_f \frac{d}{dt} \begin{bmatrix} v_{c,d} \\ v_{c,q} \end{bmatrix} + \omega C_f \begin{bmatrix} v_{c,d} \\ -v_{c,q} \end{bmatrix} + \begin{bmatrix} i_{mc,d} \\ i_{mc,q} \end{bmatrix} \quad (4\text{-}9)$$

$$C_f \frac{d}{dt} \begin{bmatrix} v_{c,d} \\ v_{c,q} \end{bmatrix} = \begin{bmatrix} i_{L,d} \\ i_{L,q} \end{bmatrix} - \begin{bmatrix} i_{mc,d} \\ i_{mc,q} \end{bmatrix} - \omega C_f \begin{bmatrix} v_{c,d} \\ -v_{c,q} \end{bmatrix}$$

$$C_f \frac{d}{dt} \begin{bmatrix} v_{c,d} \\ v_{c,q} \end{bmatrix} = \begin{bmatrix} i_{L,d} \\ i_{L,q} \end{bmatrix} - \begin{bmatrix} i_{mc,d} \\ i_{mc,q} \end{bmatrix} + \omega C_f \begin{bmatrix} -v_{c,d} \\ v_{c,q} \end{bmatrix} \quad (4\text{-}10)$$

The phrase $\omega C_f \begin{bmatrix} -v_{c,d} \\ v_{c,q} \end{bmatrix}$ and $\begin{bmatrix} i_{L,d} \\ i_{L,q} \end{bmatrix}$ are cross-coupling terms in equation (4-10). The bloack diagrm of the equation (4-10) is displayed in Figure 4.8.

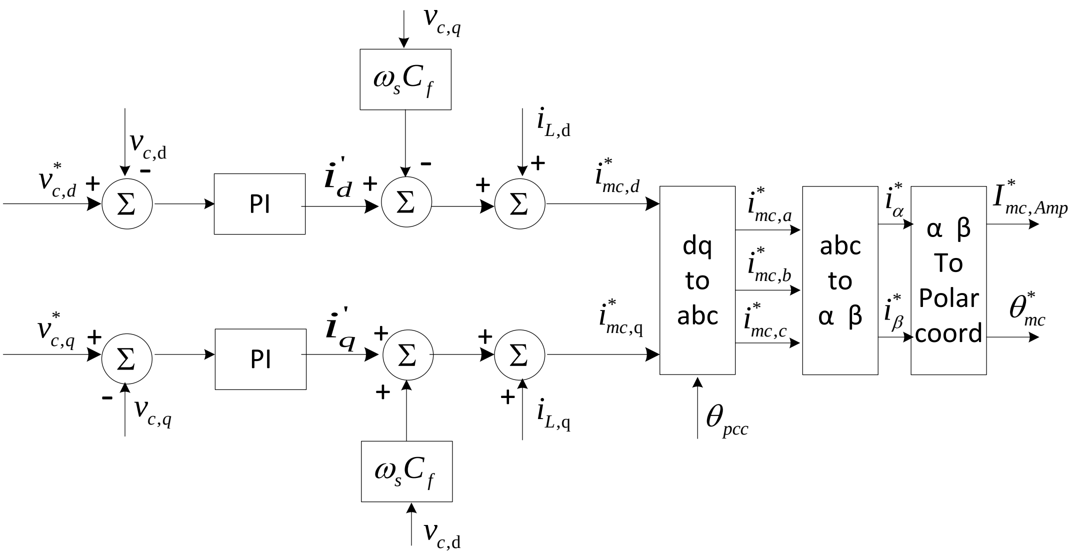


Figure 4.8 Block diagram of voltage control and dq-abc, abc-αβ and αβ-polar coordinate transformation

### 4.2.1 Designing the PI controller for the voltage-control (outer) loop

The gain $k_C$ and the time constant $T_C$ of the PI controller for the voltage control loop can be found by simplifying equation (4-10) into equation (4-11), that is by neglecting the cross coupling terms $\begin{bmatrix} i_{L,d} \\ i_{L,q} \end{bmatrix}$ and $\omega C_f \begin{bmatrix} -v_{c,d} \\ v_{c,q} \end{bmatrix}$.

$$C_f \frac{d}{dt} \begin{bmatrix} v_{c,d} \\ v_{c,q} \end{bmatrix} = - \begin{bmatrix} i_{mc,d} \\ i_{mc,q} \end{bmatrix} \quad (4\text{-}11)$$

Taking the transfer function of the d-coordinate in equation (4-11) results to:

$$C_f v_{c,d}\, s = -i_{mc,d} \tag{4-12}$$

$$H(s) = \frac{v_{c,d}}{v_{c,d}^*} = \frac{1}{C_f s} \tag{4-13}$$

The voltage control loop and the equation (4-13) can be described in the form of Figure 4.9.

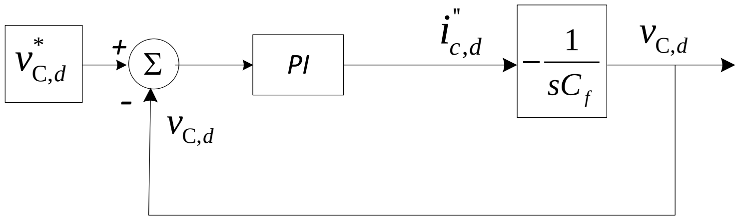


Figure 4.9 Block diagram of voltage control (inner) loop

Taking the transfer function of the voltage control loop in Figure 4.9 result to

$$H(s) = \frac{v_{c,d}}{v_{c,d}^*} = -\frac{k_C}{T_C C_f}\left(\frac{1 + T_C s}{s^2 - \frac{k_C}{C_f}s - \frac{k_C}{T_c C_f}}\right) \tag{4-14}$$

Equation above can be expressed as:

$$H(s) = \omega_{0,C}^2 \left(\frac{1 + T_C s}{s^2 + 2\xi\omega_{0,C}\, s + \omega_{0,C}^2}\right) \tag{4-15}$$

Selecting the bandwidth $\omega_{0,C}$ of the voltage control (inner) loop ten times "10" the current control outer loop's bandwidth $\omega_{0,L}$, it becomes $\omega_{0,C} = \omega_{0,L} * 10 = 628.318 * 10 = 6283.18\, rad/s$.

The gain $k_C$ and the time constant $T_C$ for the voltage control can be found as follows [16] [17]:

$$2\xi\omega_{0,C} = -\frac{k_C}{C_f}$$

$$k_C = -2\xi\omega_{0,C}\, C_f = 2 * 0.7071 * 6283.18 * 1 * 10^{-6} = -0.00888 \tag{4-16}$$

$$\omega_{0,C}^2 = -\frac{k_C}{T_c C_f} = -\frac{-2\xi\omega_{0,C}\, C_f}{T_c C_f} = \frac{2\xi\omega_{0,C}}{T_c}$$

$$T_c = \frac{2\xi}{\omega_{0,C}} = \frac{2 * 0.7071}{6283.18} = 0.000225 \tag{4-17}$$

Simulating for the gain $k_C = -0.00888$ and time constant $T_C = 0.000225$ of the PI controller for the voltage control loop, the d- and q-coordinate current reference $i_{mc,d}^*$ and $i_{mc.q}^*$ for the outer control loop is illustrated in Figure 4.10.

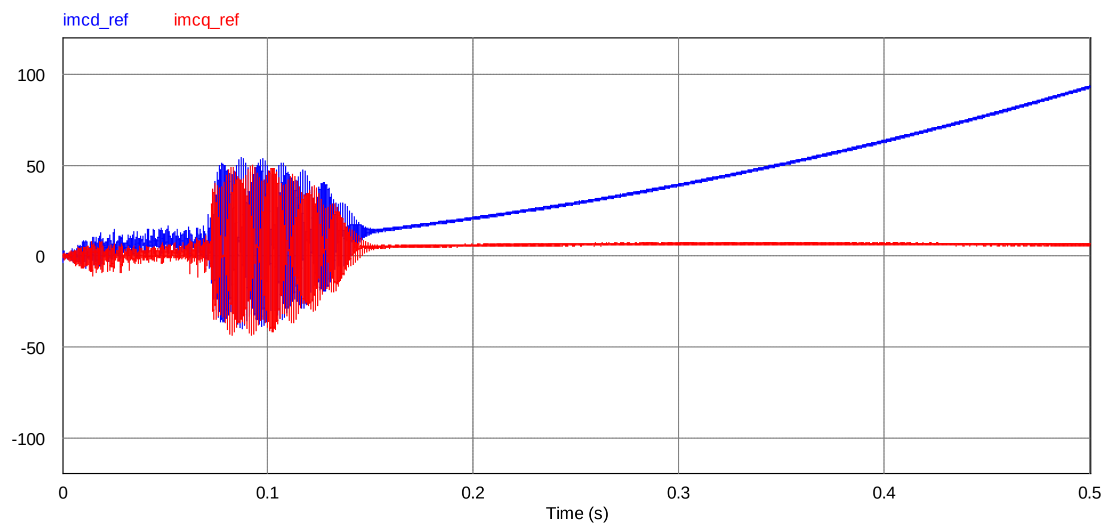


**Figure 4.10 Simulation result of current reference $i^*_{mc,d}$ and $i^*_{mc,q}$ for $k_c$ = - 0.00888 and time constant $T_C$ = 0.000225**

Figure 4.10 explain that the q-coordinate current reference (imq_ref =$i^*_{mc,q}$) in red has a constant value and it is stable. But while the d-coordinate current reference (imcd_ref = $i^*_{mc,d}$) in blue goes to plus infinity (∞) with the time, which cause the instability in the control system. This means that the gain $k_C = -0.00888$ and time constant $T_C = 0.000225$ are not the optimum values.

After many simulations by trial and error it is discovered that the proportional controller with a gain $k_C$ equal to -0.007 is the optimum value and gives stable q- and d-coordinate current reference (imq_ref = $i^*_{mc,q}$) and (imcd_ref = $i^*_{mc,d}$) respectively. This claim can be proved by simulation result in Figure 4.11.

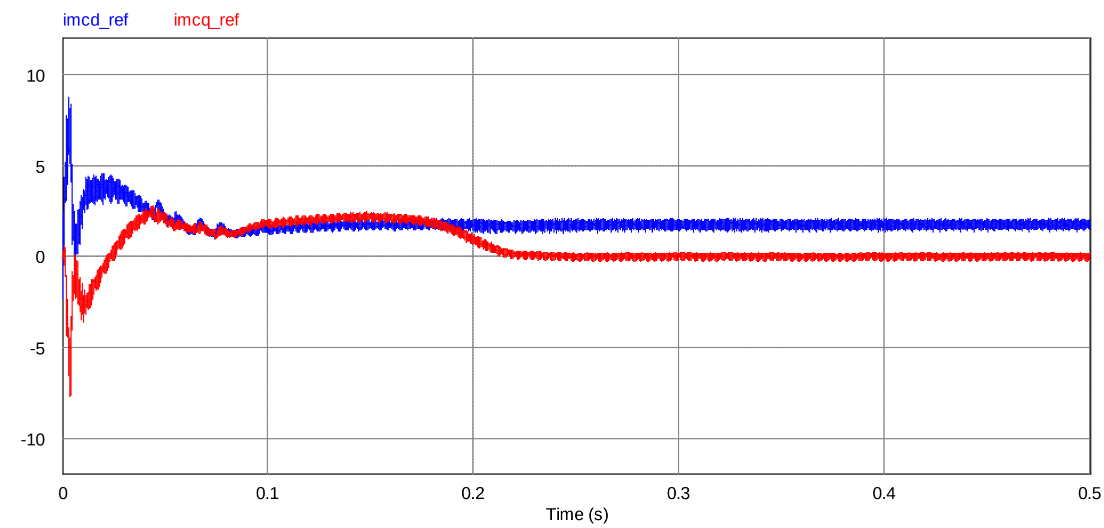


**Figure 4.11 Simulation result of current reference $i^*_{mc,d}$ and $i^*_{mc,q}$ for $k_c$ = - 0.007**

From Figure 4.7 it can be observed that the d- and q-coordinate current reference, which are (imcd_ref = $i^*_{mc,d}$) in blue and (imcq_ref = $i^*_{mc,q}$) in red are stable.

So therefore the PI controller in Figure 4.8 and Figure 4.9 have to be replace with the Proportional controller, which are represented in the form of Figure 4.12 and Figure 4.13 after replacement of the controller from PI to P.

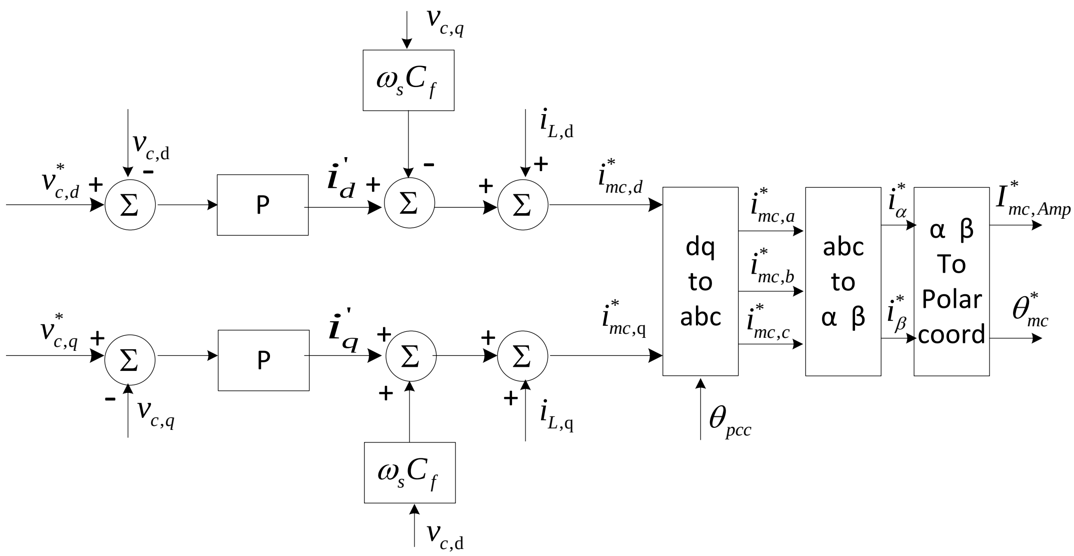


**Figure 4.12 Edited Block diagram of voltage control and dq-abc, abc-αβ and αβ-polar coordinate transformation**

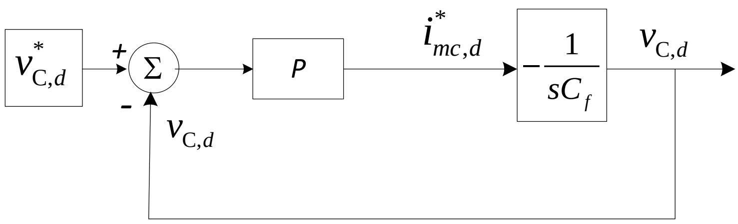


**Figure 4.13 Edited Block diagram of voltage control (inner) loop**

The current references $i^*_{mc,d}$ and $i^*_{mc,d}$ are then transformed from dq- to abc-coordinate system based on the voltage angle reference $\theta_{pcc}$. Next the abc- is transformed to the alpha-beta coordinate system and at the end the alpha-beta-coordinate system is transformed to the polar coordinate system; $I^*_{mc,Amp}$ and $\theta^*_{mc}$. All these transformations are well described in Figure 4.12.

Figure 4.14 shows the combinations of Figure 4.3, Figure 4.4 and Figure 4.12, and gives a general outlook of the 3-phase LC-filter control system.

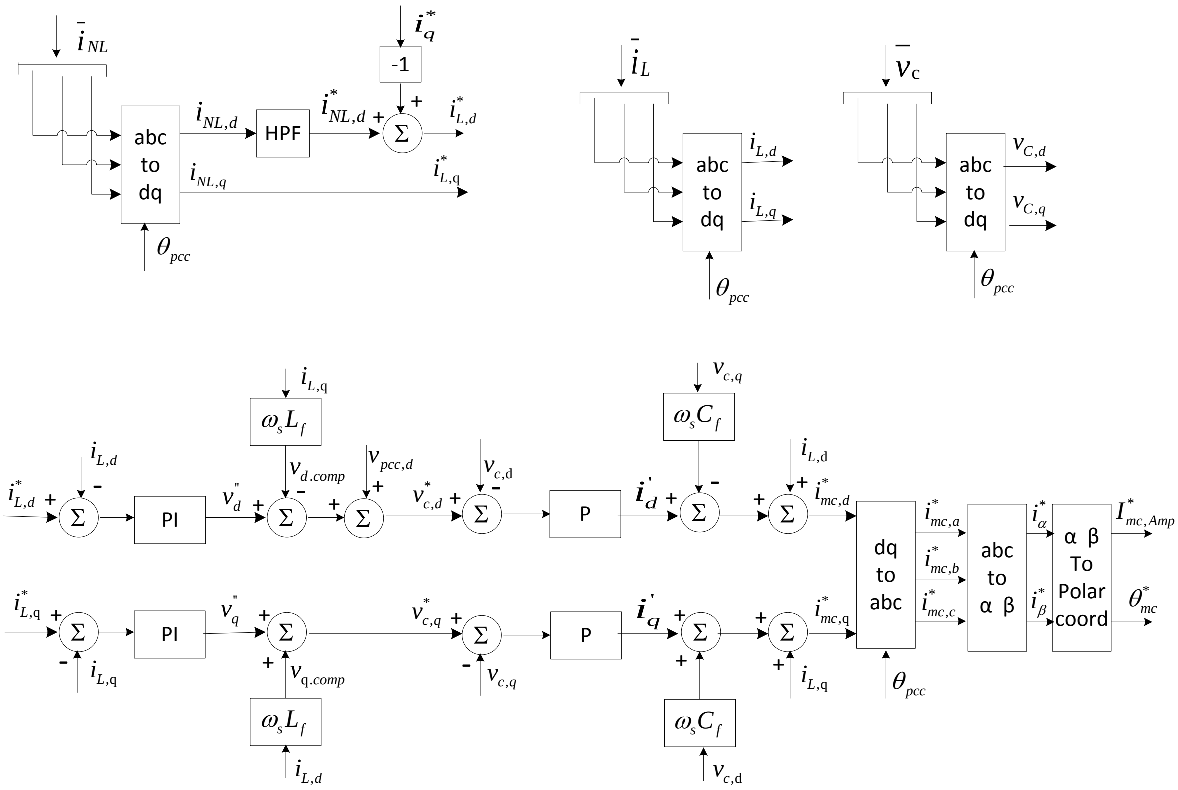


Figure 4.14 Overview of the block diagram for current-control, voltage-control and dq-abc, abc-αβ and αβ-polar coordinate transformation

The angle reference $\theta_{mc}^{*}$ obtained from polar coordinate as described in Figure 4.14 is feed to the indirect space vector modulation block wheras the current amplitude $I_{mc,Amp}^{*}$ is not in use. The angle $\theta_{mc}^{*}$ controls the harmonic and the reactive current injection to the point of common coupling.

At the same time the angle $\theta_{mc}^{*}$ also control the active current flow through the matrix converter for the PMSM.

# Chapter 5
# Simulation Results

In this chapter the simulation model of the systems described in Figure 5.1 for the matrix converter shunted with the nonlinear load and the simulation model of the system displayed in Figure 5.2 for the Back-to-Back voltage source converter shunted with the nonlinear load are built in PSIM Professional Version 9.0.6.400.

The focus of this chapter is to compare the matrix converter with the Back-to-Back voltage source converter in term of active filtering while both are shunted with the nonlinear load. And to see which one of them have a good capability to compensate and to cope with harmonics in Smart Grids.

In section 5.1 shows the simulation result for the matrix converter shunted with nonlinear load which is depicted in Figure 5.1

Whereas in section 5.2 shows the simulation results of the Back-to-Back voltage source converter shunted with the nonlinear load which is depicted in Figure 5.2.

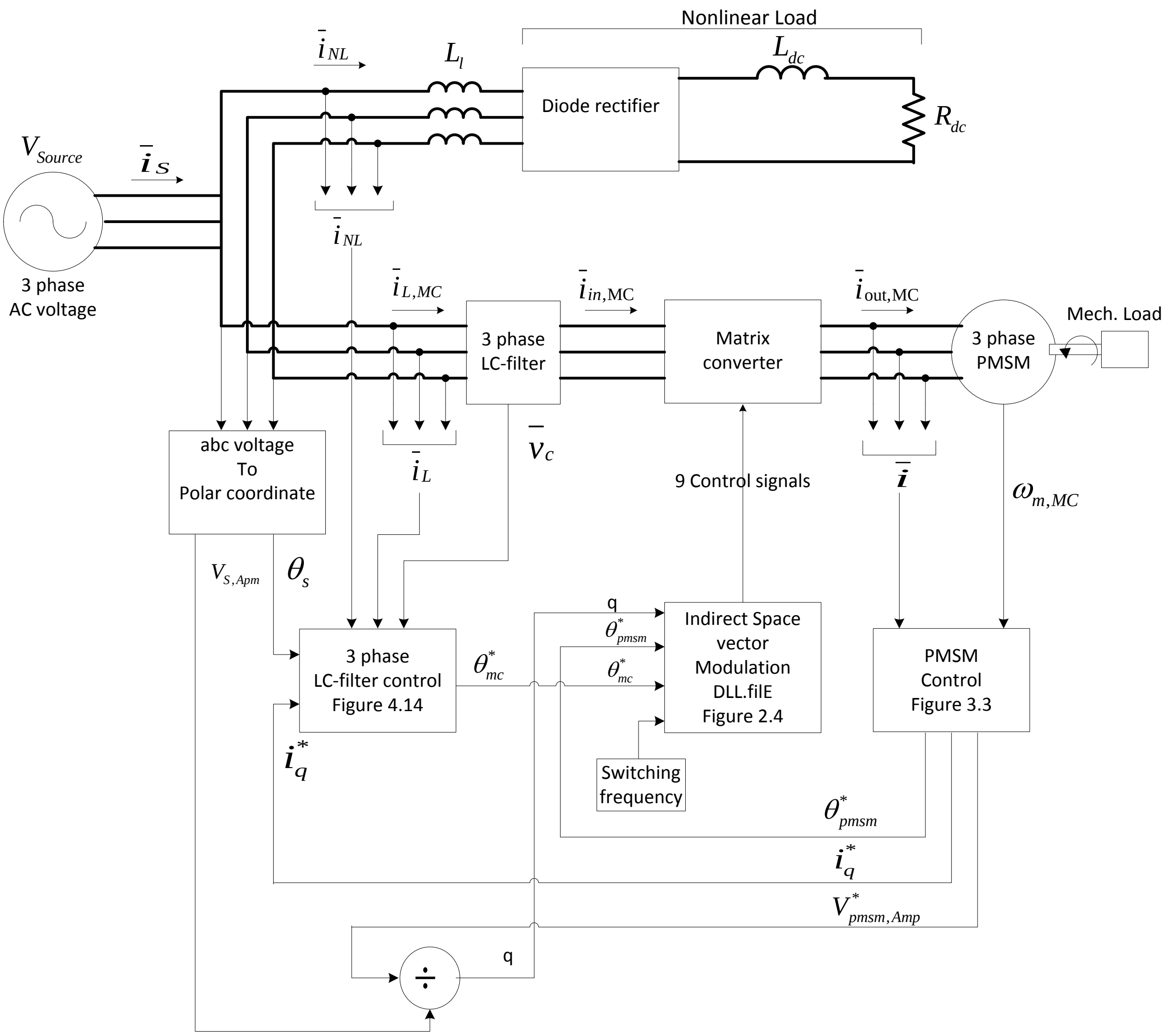


Figure 5.1 system overview of the Matrix converter shunted with the nonlinear load

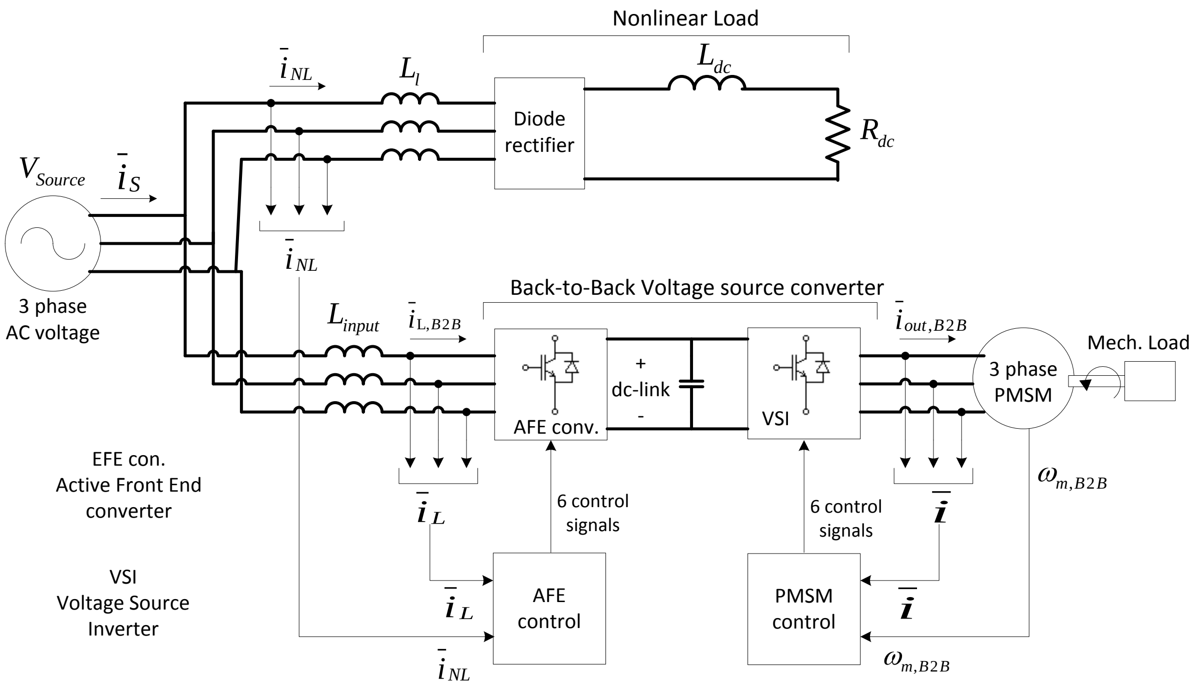


Figure 5.2 system overview of the Back-to-Back voltage source converter shunted with nonlinear load

## 5.1 Simulation results of the matrix converter shunted with nonlinear load

The indirect space vector modulation of the matrix is compiled by DLL file, therefore the PSIM require that the Microsoft Visual C++ 2010 Express should also be installed on a computer where the simulation model of Figure 5.1 is run. Table 5-1, Table 5-2 and Table 5-3 show the simulation parameter for the matrix converter.

**Table 5-1 Simulation parameters**

| Parameter | Definition | Value |
|---|---|---|
| $V_{source}$ (line-line, rms) | Source line-line rms voltage | 400 [V] |
| $F_{switching}$ | Switching frequency of the MC | 10 [kHz] |
| $P_{linear}$ (PMSM) | Rated power of PMSM | 785 [W] |
| $P_{nonlinear}$ | Rated power of nonlinear load | 1943 [W] |
| $R_{dc}$ | Resistor on the dc side of Nonlinear load | 150 [Ω] |
| $L_{dc}$ | Inductor on the DC side of the Nonlinear load | 2 [mH] |
| $L_l$ | Input line inductor of the Nonlinear load | 0.5 [mH] |
| $\omega^* = \omega_{ref}$ | Rated speed of the PMSM | 157 [rad/s] |
| $T_{Mech.load}$ | Rated torque of the mechanical load | 5 [Nm] |
| $L_f$ | Input inductor of the LC-filter of the MC | 30 [mH] |
| $C_f$ | Input capacitor of the LC-filter of the MC | 1 [µF) |

**Table 5-2 Simulation parameters for the PI controllers of PMSM control “Figure 3.3”**

| Speed-control (outer) loop “PI controller” | | Current-control (inner) loop “PI controller” | |
|---|---|---|---|
| k | 0.0622 | k | 44.38 |
| T | 0.0225 | T | 0.0022 |

**Table 5-3 Simulation parameter for the PI and P controller of the shunt active and 3-phase LC filter control “Figure 4.14”**

| Current control (outer) loop “PI controller” | | Voltage control (inner) loop “P controller” | |
|---|---|---|---|
| k | -0.5 | k | -0.007 |
| T | 0.045 | | |

The simulation assumes that the switches used in matrix converter are an ideal bidirectional switches and with zero time commutation. The rated power of the PMSM is 40.4 % of the rated power of the nonlinear load. The time step for the simulations is selected to be 0.5 µs and it is simulated for a time interval of 0.3 s.

Figure 5.3 shows the simulation results for the mechanical speed of the PMSM $\omega_m$ in red and the rated mechanical speed $\omega_{ref} = 157\, rad/s$ in blue.

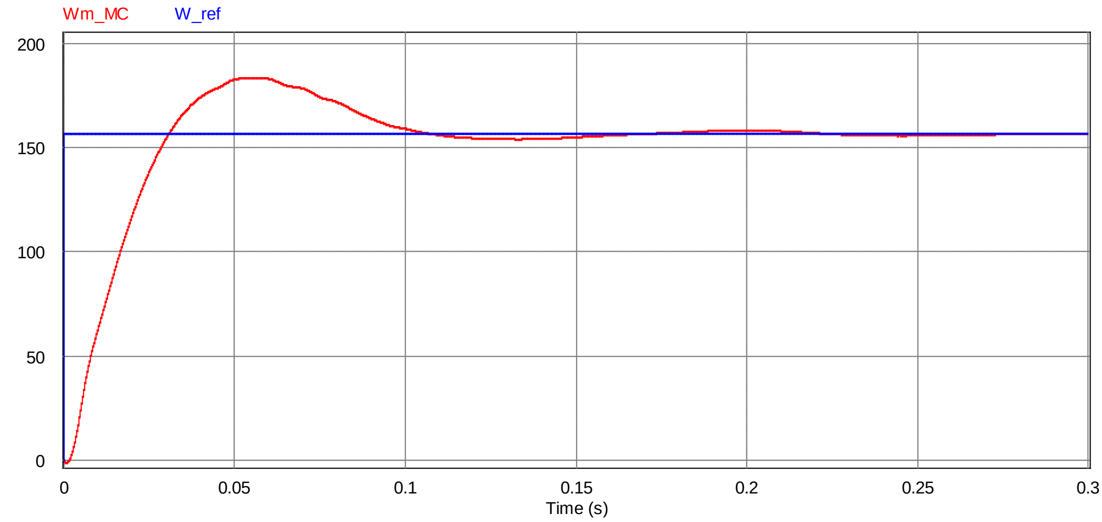


**Figure 5.3 Simulation result of rated speed $\omega_{ref}$ in blue and the mechanical speed $\omega_m$ in red for the MC as an ASD**

As the mechanical speed $\omega_m$ follow the reference/rated speed, therefore this validates the matrix converter to behave perfectly as an adjustable speed drive.

Figure 5.4 depict the output and input: voltage (blue) and current (red) for the rated speed of 157 rad/s. This figure is further zoomed and exhibited in the form of Figure 5.5.

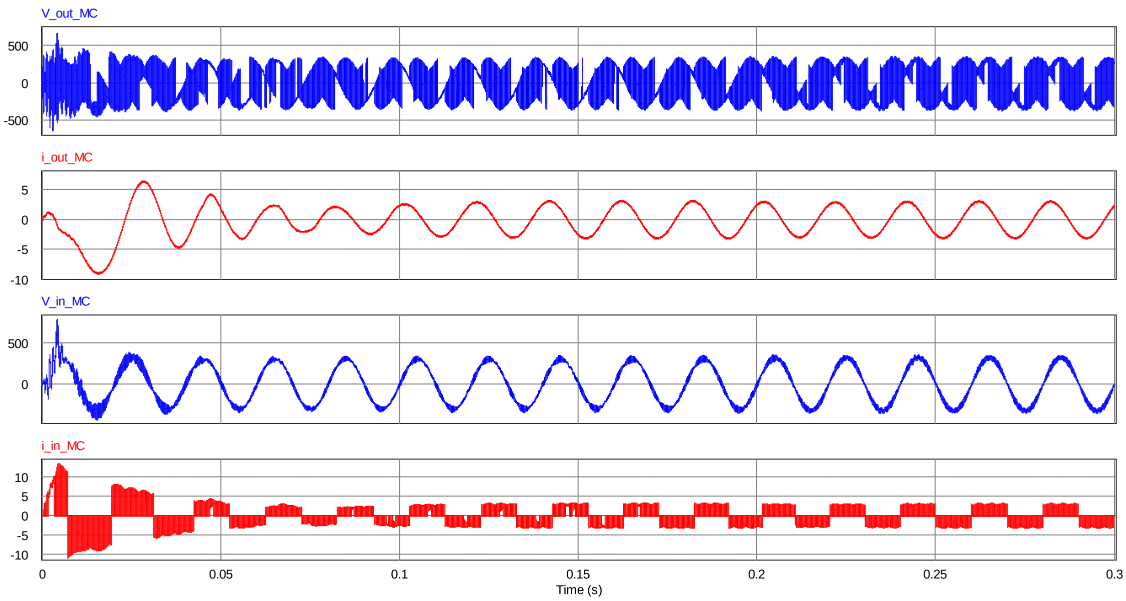


**Figure 5.4 Output voltage and current on the upper two curves and the input voltage and current in the bottom two curves**

From Figure 5.4 and Figure 5.5 this can be seen that, the output voltage and the input current contain switching pulses, this shows the output side of the matrix converter behaves as a voltage source while on the input side it behaves as a current source converter, which confirms and agrees with the reference [10].

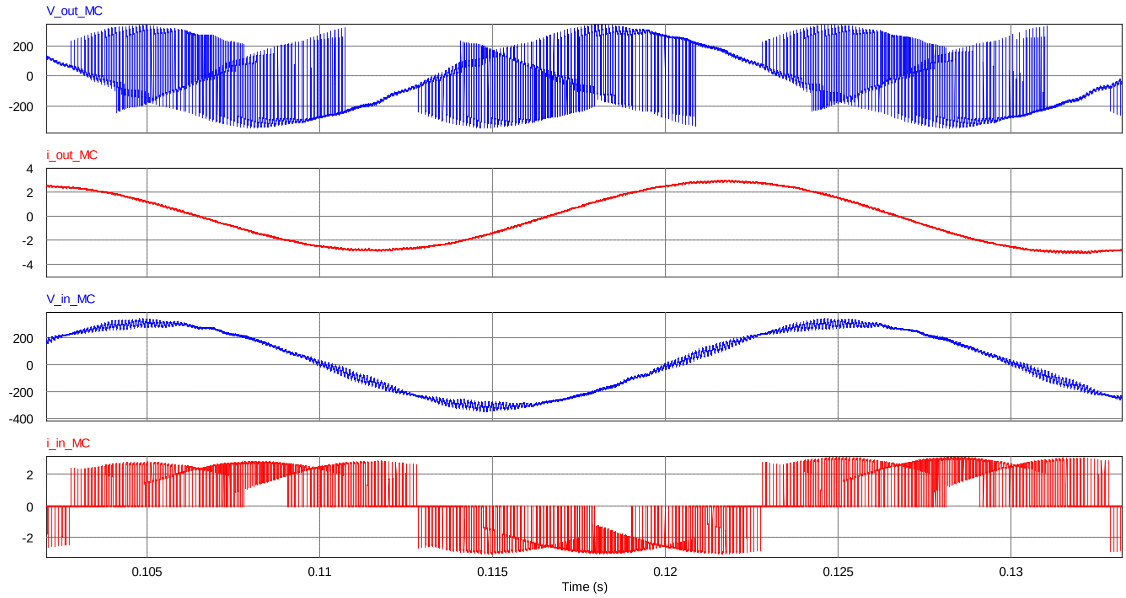


Figure 5.5 Zoomed output voltage and current and the input voltage and current

Figure 5.6 shows the nonlinear current (i_NL = $i_{NL}$) of the nonlinear load in green, the shunt active power filter current (i_L_MC = $i_{L,MC}$) in blue, and the source current i_S = $i_S$ in red.

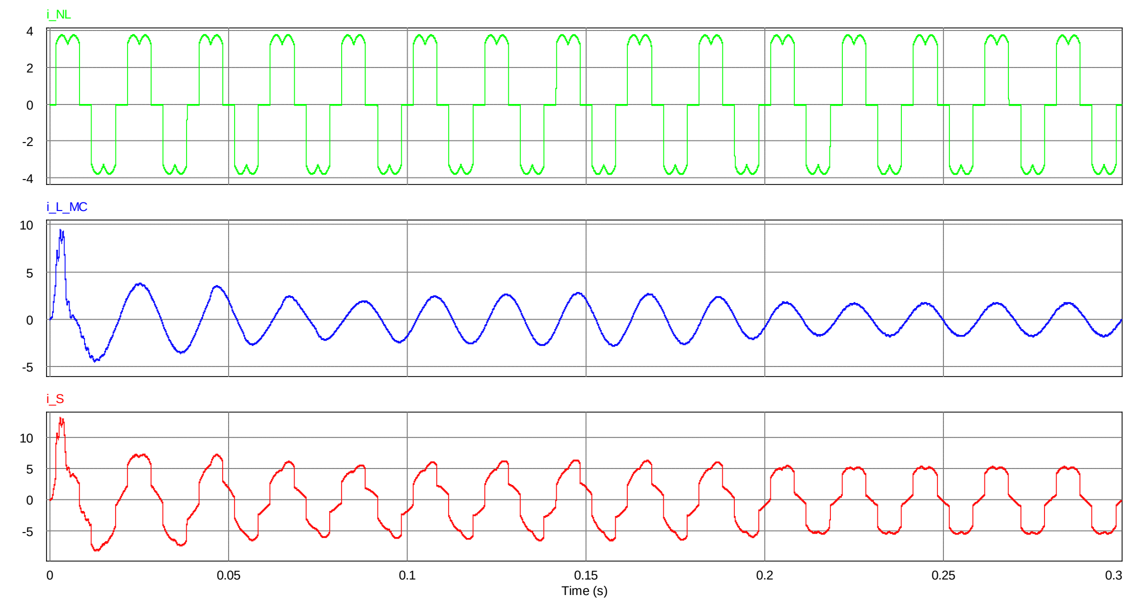


Figure 5.6 Simulation result of the nonlinear load current ( i_NL) in green, shunt active filtering current of the MC (i_L_MC) in blue and the source current ( i_S) in red for the MC

From the curve of the nonlinear current "i_NL" in Figure 5.6 and Figure 5.7, it is obvious that the nonlinear load produces harmonics current which is injected into the system. And the shunt active power filter current "i_L_MC" is supposed to compensate the harmonic current "i_NL", and make the source current "i_S" sinusoidal. But the simulation results in Figure 5.6 and Figure 5.7 shows that the source current "i_S" contains harmonics and it is not sinusoidal. This harmonic content in the source current is due to the harmonic current infiltration from the nonlinear load to the source side. The harmonic current infiltration to the source side is in consequence of poor/weak harmonic current compensation from the shunt active power filter side.

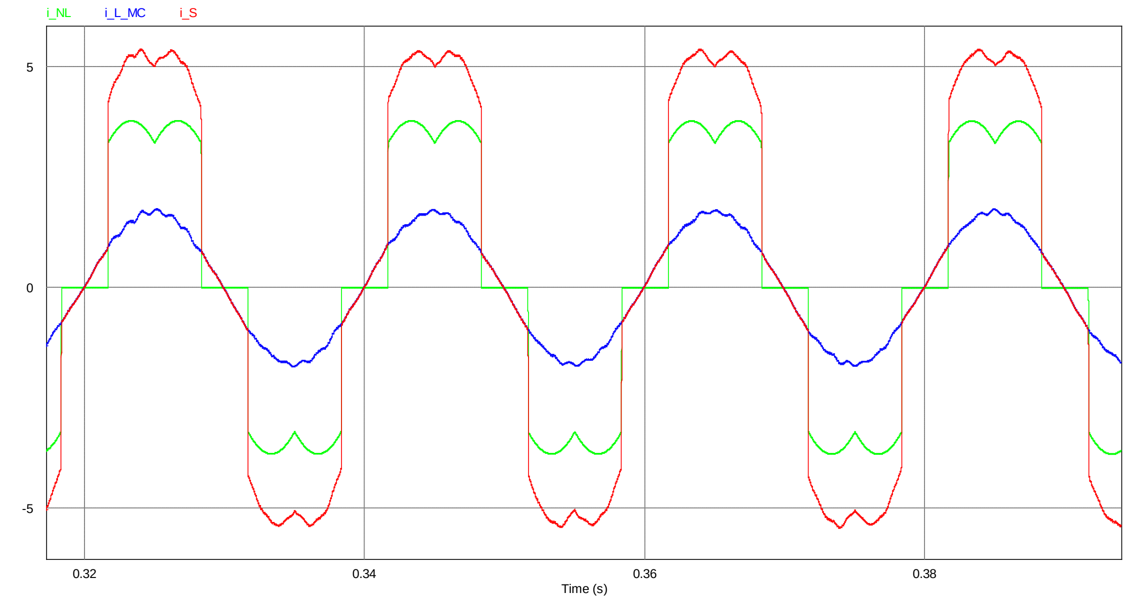


**Figure 5.7 Zoomed and combined simulation result of the nonlinear load current ( i_NL) in green, shunt active filtering current of the MC (i_L_MC) in blue and the source current ( i_S) in red for the MC**

The power factor in steady state for the source current and source voltage for the matrix converter shunted to the nonlinear load is 97.7 %. This is also depicted in Figure 5.8 and Figure 5.9.

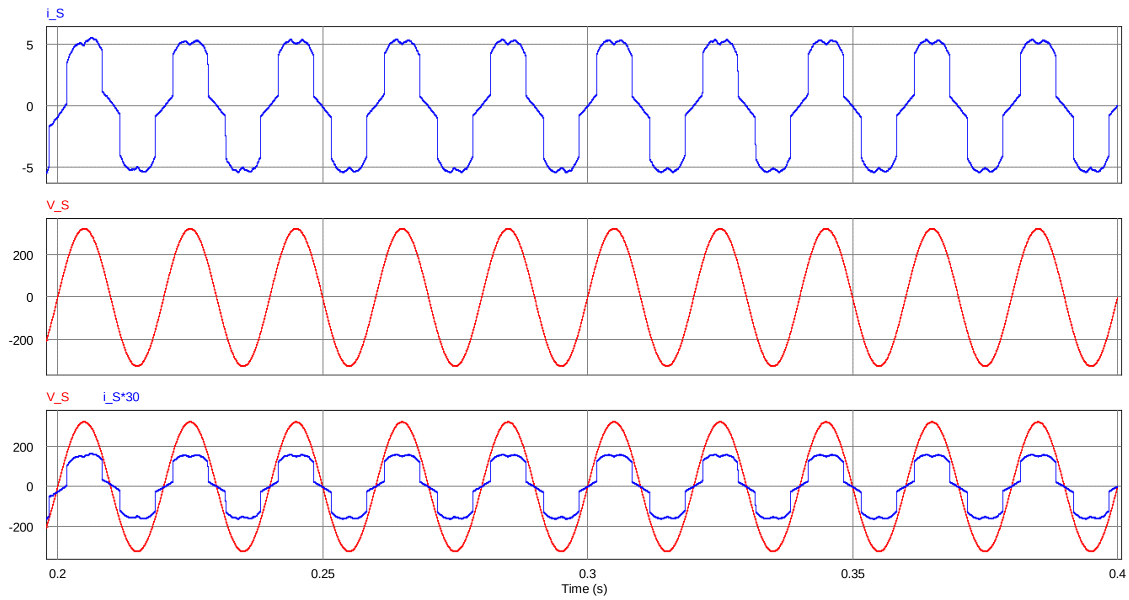


**Figure 5.8 Source current and source voltage for the matrix converter shunted to the nonlinear load**

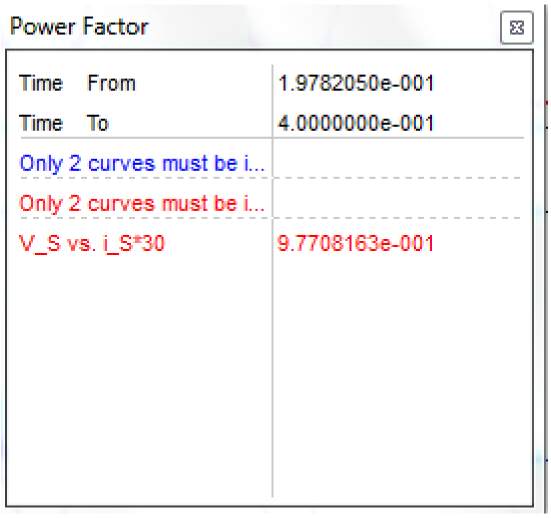


Figure 5.9 Power factor

## 5.2 Simulation results of the Back-to-Back voltage source converter shunted with nonlinear load

The design of the control system for the PMSM and AFE converter for the Back-to-Back voltage source converter is performed in the specialization project "Coping with Harmonics in Smart Grids: Analysis of the Back-to-Back converter" by Lucie Boniface or [7]. The simulation time for the simulation is 2 µs. Table 5-4, Table 5-5 and Table 5-6 present the simulation parameter for the Back-to-Back voltage source converter.

**Table 5-4 simulation parameter for the Back-to-Back voltage source converter shunted with nonlinear load**

| Parameter | Definition | Value |
|---|---|---|
| $V_{source}$ (line-line, rms) | Source line-line rms voltage | 400 [V] |
| $P_{linear}$ (PMSM) | Rated power of PMSM | 785 [W] |
| $P_{nonlinear}$ | Rated power of nonlinear load | 1943 [W] |
| $R_{dc}$ | Resistor on the dc side of Nonlinear load | 150 [Ω] |
| $L_{dc}$ | Inductor on the DC side of the Nonlinear load | 2 [mH] |
| $L_l$ | Input line inductor of the Nonlinear load | 0.5 [mH] |
| $\omega^* = \omega_{ref}$ | Rated speed of the PMSM | 157 [rad/s] |
| $T_{Mech.load}$ | Rated torque of the mechanical load | 5 [Nm] |
| $F_{AFE,\ switching}$ | Switching frequency of the AFE converter | 50 [kHz] |
| $F_{VSI,\ Switching}$ | Switching frequency of VSI | 1 [kHz] |
| $L_{input}$ | Input inductor of the Back-to-Back converter | 6 [mH] |
| $C_{DC}$ | DC-link capacitor | 60 [µF] |

**Table 5-5 Simulation parameters for the PI controllers of PMSM control**

| Speed-control (outer) loop "PI controller" | | Current-control (inner) loop "PI controller" | |
|---|---|---|---|
| k | 0.03 | k | 14 |
| T | 0.15142 | T | 0.004 |

**Table 5-6 Simulation parameter for the PI controller of the Active Front End converter**

| DC-voltage control (outer) loop "PI controller" | | Current control (inner) loop "PI controller" | |
|---|---|---|---|
| k | -0.03 | k | 480 |
| T | 0.005 | T | 0.000026 |

Figure 5.10 depict the simulation results for the mechanical speed of the PMSM $\omega_m$ in red and the rated mechanical speed $\omega_{ref} = 157\ rad/s$ in blue.

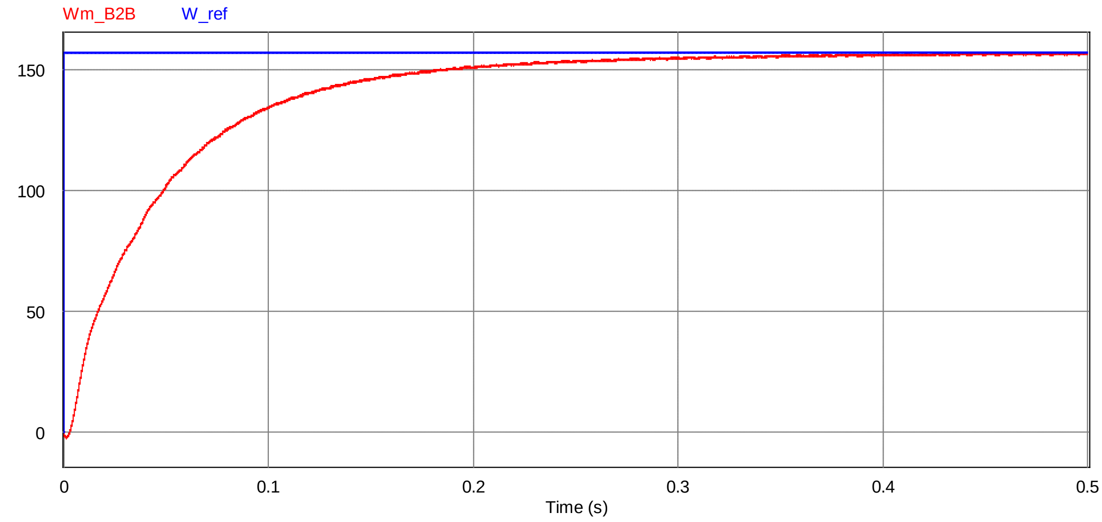


**Figure 5.10 Simulation result of rated speed $\omega_{ref}$ in blue and the mechanical speed $\omega_m$ in red for the B2B converter as an ASD**

From the figure above it can be seen that the mechanical speed follow the reference/rated speed; therefore the Back-to-Back voltage source converter behaves as a perfect adjustable speed drive.

Figure 5.11 illustrate the nonlinear current (i_NL = $i_{NL}$) of the nonlinear load in green, the shunt active power filter current (i_L_B2B = $i_{L,B2B}$) in blue, and the source current i_S = $i_S$ in red for the Back-to-Back voltage source converter as an adjustable speed drive and shunt active power filter.

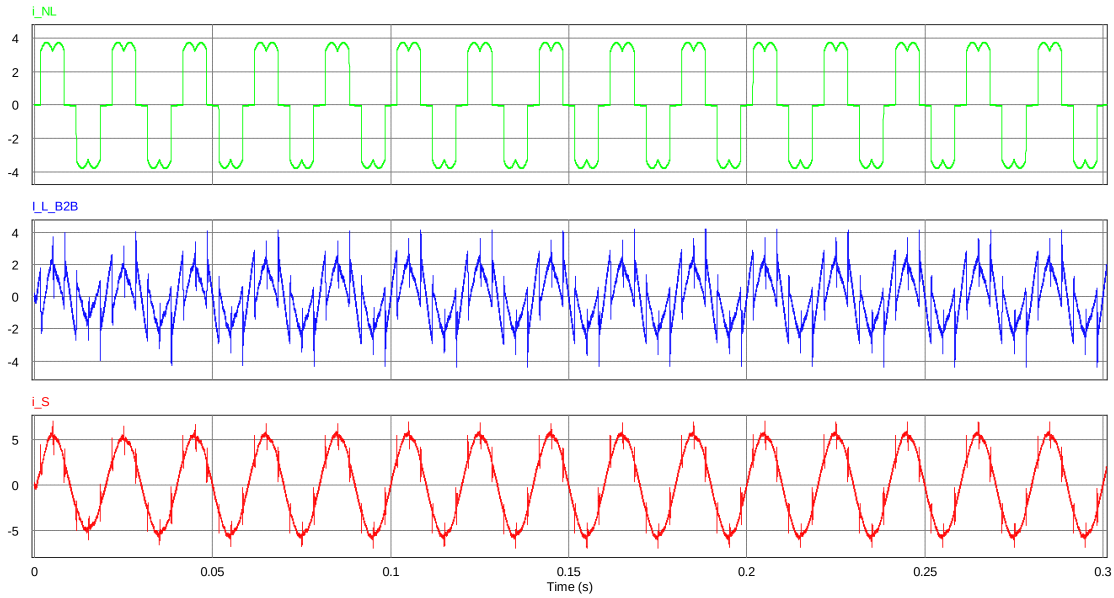


**Figure 5.11 Simulation result of the nonlinear load current ( i_NL) in green, shunt active power filter current of the B2B converter (i_L_B2B) in blue and the source current ( i_S) in red**

From the curve of the nonlinear current "i_NL" in Figure 5.11 and Figure 5.12, it is obvious that the nonlinear load produces a harmonic which is injected into the system. The Back-to-Back voltage source converter which behaves as a shunt active power filter compensates the harmonic current i_NL by injecting the current "i_L_B2B" to the system. As a consequence source current i_S becomes sinusoidal.

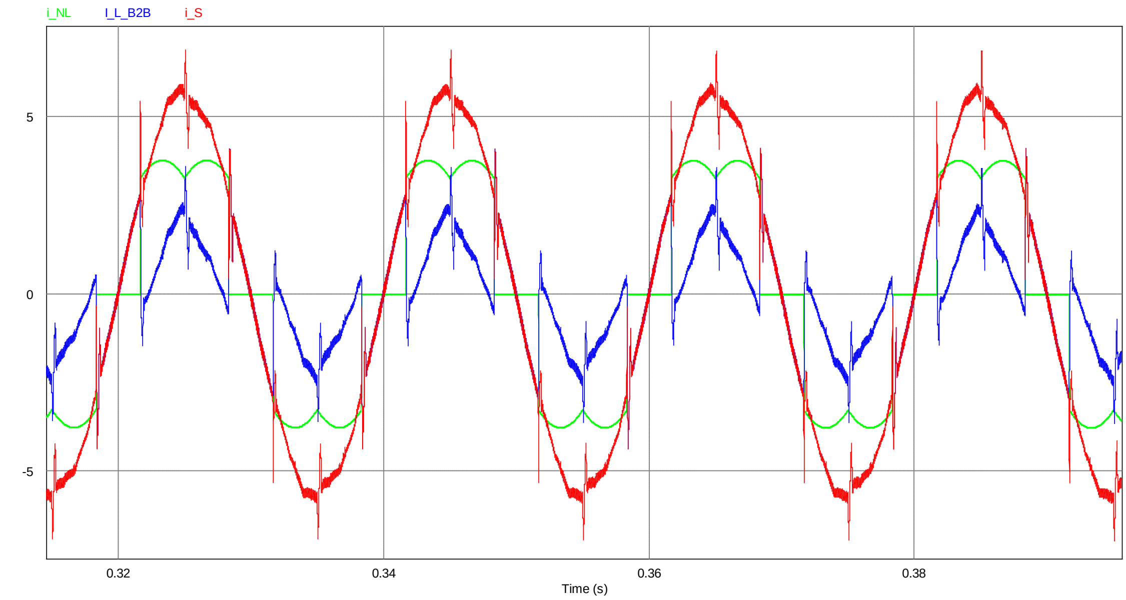


**Figure 5.12 Zoomed and combined simulation result of the nonlinear load current ( i_NL) in green, shunt active filtering current of the MC (i_L_B2B) in blue and the source current ( i_S) in red for the B2B converter**

The power factor in steady state for the source current and source voltage for the Back-to-Back voltage source converter shunted to the nonlinear load is 99.72 %. This is also depicted in Figure 5.13 and Figure 5.14

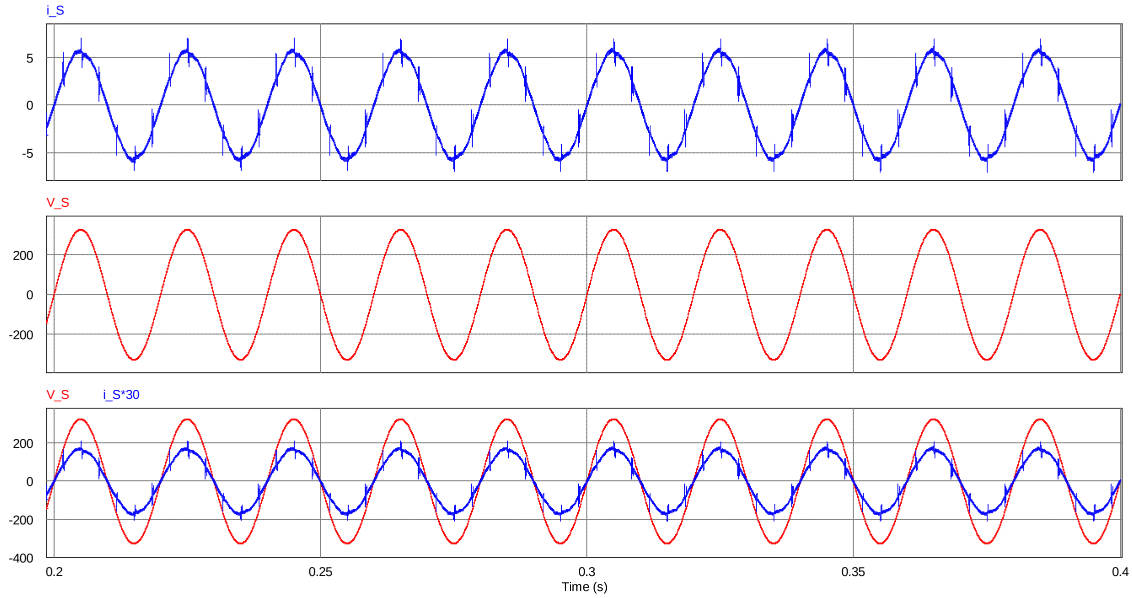


**Figure 5.13 Source current and voltage for Back-to-Back voltage source converter shunted to the nonlinear load**

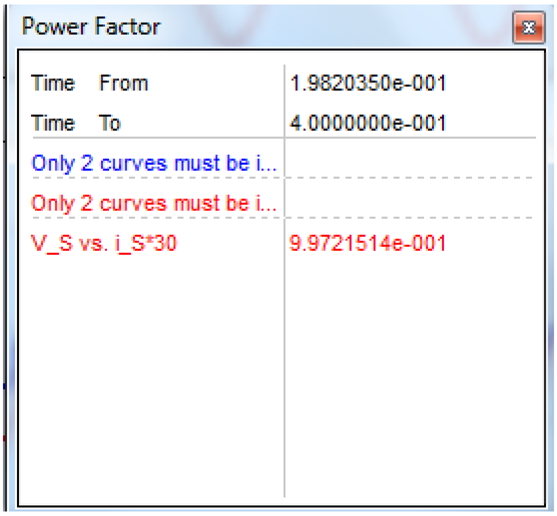


Figure 5.14 Power factor

# Chapter 6
# Discussion

From the simulation results of the matrix converter in section 5.1 it is evident and fair to assert that the matrix converter does not have the active filtering capability at all, when it is operating as an adjustable speed drive for the PMSM or any other motor. The reasons that the matrix cannot operates/functions as an active filter while it is interfaced as an adjustable speed drive between the PMSM and the voltage source, are as follows:

I. It does not has reactive energy storage component like DC-link capacitor and inductor
II. The instantaneous input power is equal to the instantaneous output power
III. The input current of the matrix converter contain/consist of switching pulses
IV. Permanent magnet synchronous machine behave as an electrical load, which further operates as an active and reactive power sink, this cause absorption and consumption of active and reactive power from source.

And from the simulation results of the Back-to-Back voltage source converter in section 5.2, it is obvious that the Back-to-Back converter has an excellent active filtering capability and reactive power compensation. The reasons for excellent active filtering are as follows:

I. It has reactive energy storage component like DC-link capacitor which separates the voltage source inverter from the active front end filter.
II. The reactive energy stored in DC-linked capacitor can supply the reactive power to the motor for magnetization and to the nonlinear load for harmonic and reactive power compensation.
III. The instantaneous input power is not equal to the instantaneous output power
IV. Both the voltage source inverter and the Active front end filter each have its own control system and they are independent of each other.

Having the reactive energy storage component is one of the conditions for the active filtering and in addition it also gives better reactive power compensation.

# Chapter 7
# Conclusion

In this master thesis it was investigated to find out, if the matrix converter has the capability to compensate the harmonic current, while it is operating as a variable speed drive. And to compare it with the Back-to-Back voltage source converter in term of active filtering.

To use the matrix converter as a motor drive and a shunt active power filter the control systems for the PMSM, shunt active power filter and 3-phase LC-filter were built.

The simulation results shows that the matrix converter with the presented control strategy cannot perform two functions at the same time, those are:

a) To behave as a variable speed drive
b) To act as a shunt active power filter

The reasons that the matrix converter cannot operate as a shunt active power filter are; in matrix converter the instantaneous input power is equal to the instantaneous output power, and it does not has energy storage component like DC-link capacitor or inductor.

In other word it can be described as, in case of the matrix converter the instantaneous input active and reactive power is consumed and absorbed instantaneously by the motor

Therefore it can be concluded that the Back-to-Back voltage source converter is the best in the term of active filtering and to cope with the harmonic in smart grids. On the other hand the matrix converter cannot cope with the harmonics in smart grids.

## 7.1 Future work

It seems that the presented control strategy for the PMSM and 3-phase LC-filter are not appropriate for active filtering. Therefore for the future work it can be suggested to try with the predictive control strategy both for PMSM and 3-phase LC-filter.

# Bibliography


[1] M. Cichowlas, "PWM Rectifier with Active Filtering," Warsaw University of Technology, Warsaw, 2004.

[2] M. Peterson, B. N. Singh and P. Rastgoufard, "Active and Passive Filtering for Harmonic Compensation," in *University of New Orleans*, New Orlean, 2008.

[3] H. Akagi, "New Trends in Active Filters for Power Conditioning," *IEEE TRANSACTION ON INDUSTRY APPLICATION,* vol. 32, no. 6, p. 1312, 1996.

[4] S. Hansen, P. Nielsen and F. Blaabjerg, "Harmonic Cancellation by Mixing Non-linear Single-phase and Three-phase Loads," in *Aalborg University, Institute of Energy Technology*, Aalborg, Denmark.

[5] B. Singh, K. Al-Haddad and A. Chandra, "A Review of Active Filters for Power Quality Improvement," *IEEE TRANSACTION ON INDUSTRIAL ELECTRONICS,* vol. 46, no. 5, pp. 960-966, 1999.

[6] F. Abrahamsen and A. David, "Adjustable Speed Drive with Active filtering Capability for Harmonic Current Compensation," Aalborg University, Aalborg East.

[7] L. Boniface, "Coping with Harmonics in Smart Grid: Analysis of the Back-to-Back voltage source converter," Trondheim, 2012.

[8] J.-i. Itoh, I. Sato, A. Odak, H. Ohguchi, H. Kodatchi and N. Eguchi, "A Novel Approach to Practical Matix Converter Motor Drive System with Reverse Blocking IGBT," in *IEEE Power Electronics Specialist conference*, Aachen, Germany, 2004.

[9] N. M.-A. Holtsmark, "A Matrix converter-interfaced PM Generator System with Active Filter Capabilities," in *European Association for the Development of Renewable Energies, Enviroment and Power Quality*, Satiago de Compostela, 2012.

[10] Mohan, Undeland and Robbins, Power electronics Converters, Application And Design, JOHN WILLEY & SONS, INC., 2003.

[11] P. Wheeler and D. Grant, "Optimised input filiter desgn and low-loss switching techniques for a practical matrix converter," in *IEEE*, 1997.

[12] N. M.-A. Holtsmark, "Reactive Power Compensation using a Matrix Converter," Norwegian University of Science and Technology, Trondheim, 2010.

[13] M. Venturini and A. Alesina, "Intrinsic amplitude limits and optimum design of 9 swithces direct pwm ac-ac converters," *In Power Electronics Specialist Conference,* vol. 2, pp. 1284-1291, 1988.

[14] J. C. Wiseman, "Active Damping Control of a High-Power PWM Current-Source Rectrifier for Line-Current THD Reduction," *IEEE TRANSACTIONS ON INDUSTRIAL ELECTRONICS,* vol. 52, p. 758, 2005.

[15] N. MOHAN, ADVANCED ELECTRIC DRIVES, Analysis, Control and Modeling usning Simulink, Minneapolis: MNPERE , 2001.

[16] J. G. Balchen, T. Andressen and B. A. Foss, Reguleringsteknikk, Trondheim: Institutt for teknisk kybernetikk, NTNU, 2003.

[17] N. Hotsmark, S. Sanchez and M. Molinas, "Speed regulation of a wind turbine with current source or matrix converter: Tunin procedure".

[18] P. W. Wheeler, J. Rodi'guez and J. C. a. E. L. Clare, "Matrix Converter: A Technology Review," *IEEE TRANSACTIONS ON INDUSTRIAL ELECTRONICS,* vol. 49, 2002.

[20] A. Carlsson, "The back to back converter control and design," Lund institute of technology, Lund, Sweden, 1998.

# A. Appendix

$$\begin{bmatrix} x_d \\ x_q \end{bmatrix} = \frac{2}{3}\begin{bmatrix} \cos(\theta) & \cos\left(\theta - \frac{2\pi}{3}\right) & \cos\left(\theta + \frac{2\pi}{3}\right) \\ \sin(\theta) & \sin(\theta - \frac{2\pi}{3}) & \sin(\theta + \frac{2\pi}{3}) \end{bmatrix}\begin{bmatrix} x_a \\ x_b \\ x_c \end{bmatrix} \quad \text{(A.1)}$$

Where Park's transformation is

$$P = \frac{2}{3}\begin{bmatrix} \cos(\theta) & \cos\left(\theta - \frac{2\pi}{3}\right) & \cos\left(\theta + \frac{2\pi}{3}\right) \\ \sin(\theta) & \sin(\theta - \frac{2\pi}{3}) & \sin(\theta + \frac{2\pi}{3}) \end{bmatrix} \quad \text{(A-2)}$$

And the inverse of Park's transformation is

$$P^{-1} = \begin{bmatrix} \cos(\theta) & \sin(\theta) \\ \cos\left(\theta - \frac{2\pi}{3}\right) & \sin(\theta - \frac{2\pi}{3}) \\ \cos\left(\theta + \frac{2\pi}{3}\right) & sin\left(\theta + \frac{2\pi}{3}\right) \end{bmatrix} \quad \text{(A-3)}$$

The abc phase can be achieved again by using the invers of the Park's transformation, see equation **(4-4)**

$$\begin{bmatrix} x_a \\ x_b \\ x_c \end{bmatrix} = \begin{bmatrix} \cos(\theta) & \sin(\theta) \\ \cos\left(\theta - \frac{2\pi}{3}\right) & \sin(\theta - \frac{2\pi}{3}) \\ \cos\left(\theta + \frac{2\pi}{3}\right) & sin\left(\theta + \frac{2\pi}{3}\right) \end{bmatrix}\begin{bmatrix} x_d \\ x_q \end{bmatrix} \quad \text{(A-4)}$$

$$\begin{bmatrix} x_a \\ x_b \\ x_c \end{bmatrix} = \begin{bmatrix} \cos(\theta) & \sin(\theta) \\ \cos\left(\theta - \frac{2\pi}{3}\right) & \sin(\theta - \frac{2\pi}{3}) \\ \cos\left(\theta + \frac{2\pi}{3}\right) & sin\left(\theta + \frac{2\pi}{3}\right) \end{bmatrix}\begin{bmatrix} x_d \\ x_q \end{bmatrix} \quad \text{(A-5)}$$

$$\frac{d}{dt}\begin{bmatrix} x_a \\ x_b \\ x_c \end{bmatrix} = \frac{d}{dt}\begin{bmatrix} \cos(\theta) & \sin(\theta) \\ \cos\left(\theta - \frac{2\pi}{3}\right) & \sin(\theta - \frac{2\pi}{3}) \\ \cos\left(\theta + \frac{2\pi}{3}\right) & sin\left(\theta + \frac{2\pi}{3}\right) \end{bmatrix}\begin{bmatrix} x_d \\ x_q \end{bmatrix} + \begin{bmatrix} \cos(\theta) & \sin(\theta) \\ \cos\left(\theta - \frac{2\pi}{3}\right) & \sin(\theta - \frac{2\pi}{3}) \\ \cos\left(\theta + \frac{2\pi}{3}\right) & sin\left(\theta + \frac{2\pi}{3}\right) \end{bmatrix}\frac{d}{dt}\begin{bmatrix} x_d \\ x_q \end{bmatrix} \quad \text{(A-6)}$$

$$\frac{d}{dt}\begin{bmatrix}x_a\\x_b\\x_c\end{bmatrix}=\omega\begin{bmatrix}-\sin(\theta) & \cos(\theta)\\-\sin\left(\theta-\frac{2\pi}{3}\right) & \cos(\theta-\frac{2\pi}{3})\\-\sin\left(\theta+\frac{2\pi}{3}\right) & cos\left(\theta+\frac{2\pi}{3}\right)\end{bmatrix}\begin{bmatrix}x_d\\x_q\end{bmatrix}+\begin{bmatrix}\cos(\theta) & \sin(\theta)\\\cos\left(\theta-\frac{2\pi}{3}\right) & \sin(\theta-\frac{2\pi}{3})\\\cos\left(\theta+\frac{2\pi}{3}\right) & sin\left(\theta+\frac{2\pi}{3}\right)\end{bmatrix}\frac{d}{dt}\begin{bmatrix}x_d\\x_q\end{bmatrix}\quad(7\text{-}7)$$

$$\frac{d}{dt}\begin{bmatrix}x_a\\x_b\\x_c\end{bmatrix}=\omega\begin{pmatrix}-\sin(\theta)i_d+\cos(\theta)\,i_q\\-\sin\left(\theta-\frac{2\pi}{3}\right)i_d+\cos\left(\theta-\frac{2\pi}{3}\right)i_q\\-\sin\left(\theta+\frac{2\pi}{3}\right)i_d+\cos\left(\theta+\frac{2\pi}{3}\right)i_q\end{pmatrix}+P\frac{d}{dt}\begin{bmatrix}x_d\\x_q\end{bmatrix}\quad(A\text{-}8)$$

$$\frac{d}{dt}\begin{bmatrix}x_a\\x_b\\x_c\end{bmatrix}=\omega\begin{pmatrix}\cos(\theta)\,i_q-\sin(\theta)i_d\\\cos\left(\theta-\frac{2\pi}{3}\right)i_q-\sin\left(\theta-\frac{2\pi}{3}\right)i_d\\\cos\left(\theta+\frac{2\pi}{3}\right)i_q-\sin\left(\theta+\frac{2\pi}{3}\right)i_d\end{pmatrix}+P\frac{d}{dt}\begin{bmatrix}x_d\\x_q\end{bmatrix}\quad(A\text{-}9)$$

$$\frac{d}{dt}\begin{bmatrix}x_a\\x_b\\x_c\end{bmatrix}=\omega\begin{bmatrix}\cos(\theta) & \sin(\theta)\\\cos\left(\theta-\frac{2\pi}{3}\right) & \sin(\theta-\frac{2\pi}{3})\\\cos\left(\theta+\frac{2\pi}{3}\right) & sin\left(\theta+\frac{2\pi}{3}\right)\end{bmatrix}\begin{bmatrix}x_q\\-x_d\end{bmatrix}+P\frac{d}{dt}\begin{bmatrix}x_d\\x_q\end{bmatrix}\quad(A\text{-}10)$$

$$\frac{d}{dt}\begin{bmatrix}x_a\\x_b\\x_c\end{bmatrix}=\omega P^{-1}\begin{bmatrix}x_q\\-x_d\end{bmatrix}+P^{-1}\frac{d}{dt}\begin{bmatrix}x_d\\x_q\end{bmatrix}\quad(A\text{-}11)$$

Multiplying equation **(7-7)** with Park's transformation factor P, which result into equation

$$P\frac{d}{dt}\begin{bmatrix}x_a\\x_b\\x_c\end{bmatrix}=P\omega P^{-1}\begin{bmatrix}x_q\\-x_d\end{bmatrix}+PP^{-1}\frac{d}{dt}\begin{bmatrix}x_d\\x_q\end{bmatrix}\quad(A\text{-}12)$$

$$L_f\left(\omega P^{-1}\begin{bmatrix}i_q\\-i_d\end{bmatrix}+P^{-1}\frac{d}{dt}\begin{bmatrix}i_d\\i_q\end{bmatrix}\right)=\begin{bmatrix}v_{pcca}\\v_{pccb}\\v_{pcca}\end{bmatrix}-\begin{bmatrix}v_{ca}\\v_{cb}\\v_{cc}\end{bmatrix}\quad(A\text{-}13)$$

Multiplying equation **(7-9)** by Transformation factor T, which results to

$$L_f\left(\omega P.P^{-1}\begin{bmatrix}i_q\\-i_d\end{bmatrix}+P.P^{-1}\frac{d}{dt}\begin{bmatrix}i_d\\i_q\end{bmatrix}\right)=P\begin{bmatrix}v_{pcca}\\v_{pccb}\\v_{pcca}\end{bmatrix}-P\begin{bmatrix}v_{ca}\\v_{cb}\\v_{cc}\end{bmatrix}\quad(A\text{-}14)$$

$$L_f\omega\begin{bmatrix}i_q\\-i_d\end{bmatrix}+L_f\frac{d}{dt}\begin{bmatrix}i_d\\i_q\end{bmatrix}=\begin{bmatrix}V_{pccd}\\V_{pccq}\end{bmatrix}-\begin{bmatrix}V_{cd}\\V_{cq}\end{bmatrix}\quad(A\text{-}15)$$

The q coordinate of the voltage at the point of commo n coupling (pcc) is zero

$$L_f \frac{d}{dt}\begin{bmatrix} i_d \\ i_q \end{bmatrix} = \begin{bmatrix} V_{pccd} \\ 0 \end{bmatrix} - \begin{bmatrix} V_{cd} \\ V_{cq} \end{bmatrix} - L_f \omega \begin{bmatrix} i_q \\ -i_d \end{bmatrix} \tag{A-16}$$

# B. Appendix

## Matrix converter and its control

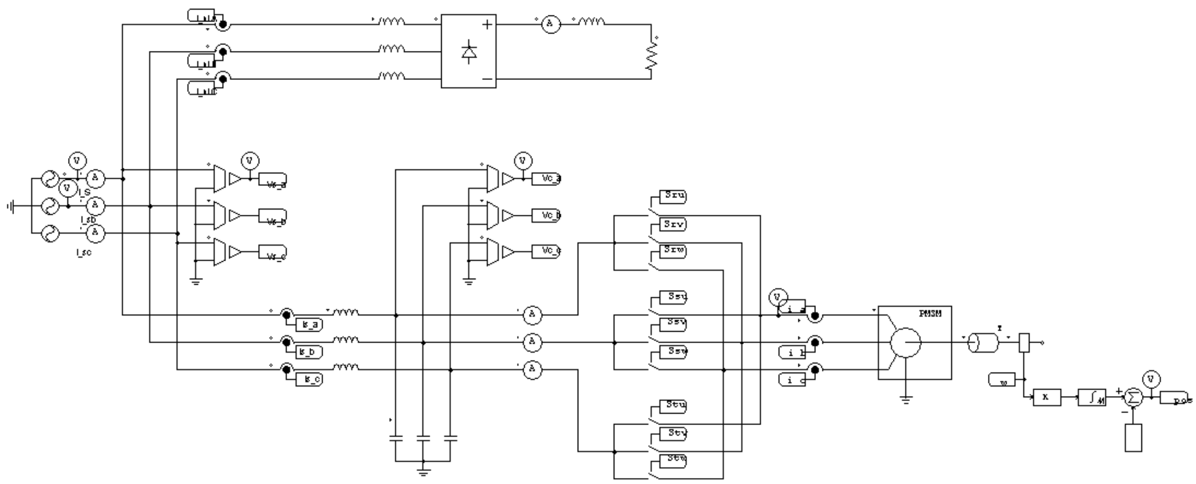

Figure B.1 Equivalent circuit of the matrix converter shunted with nonlinear load

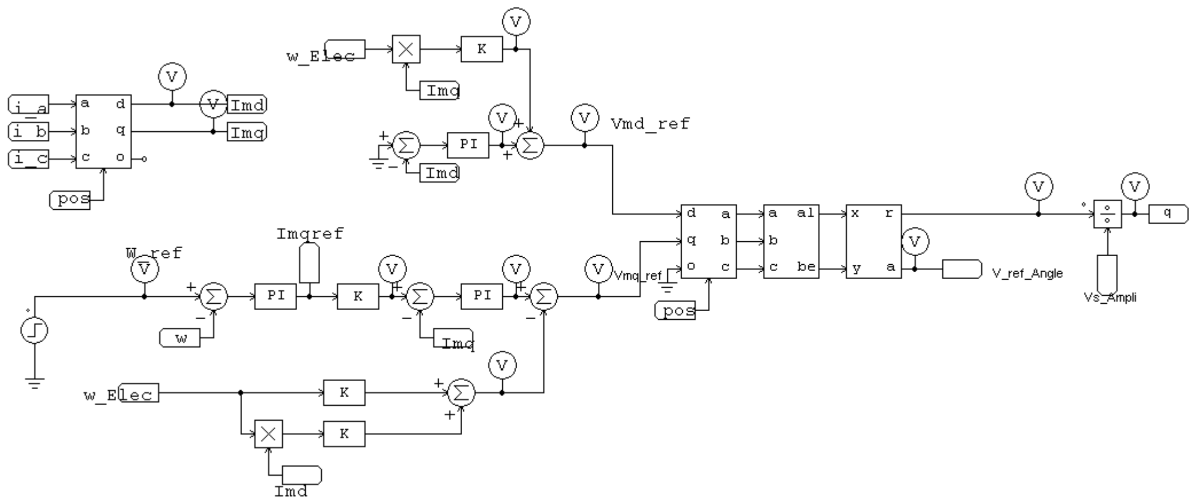


Figure B.2 Control system of the Permanent magnet synchronous machine

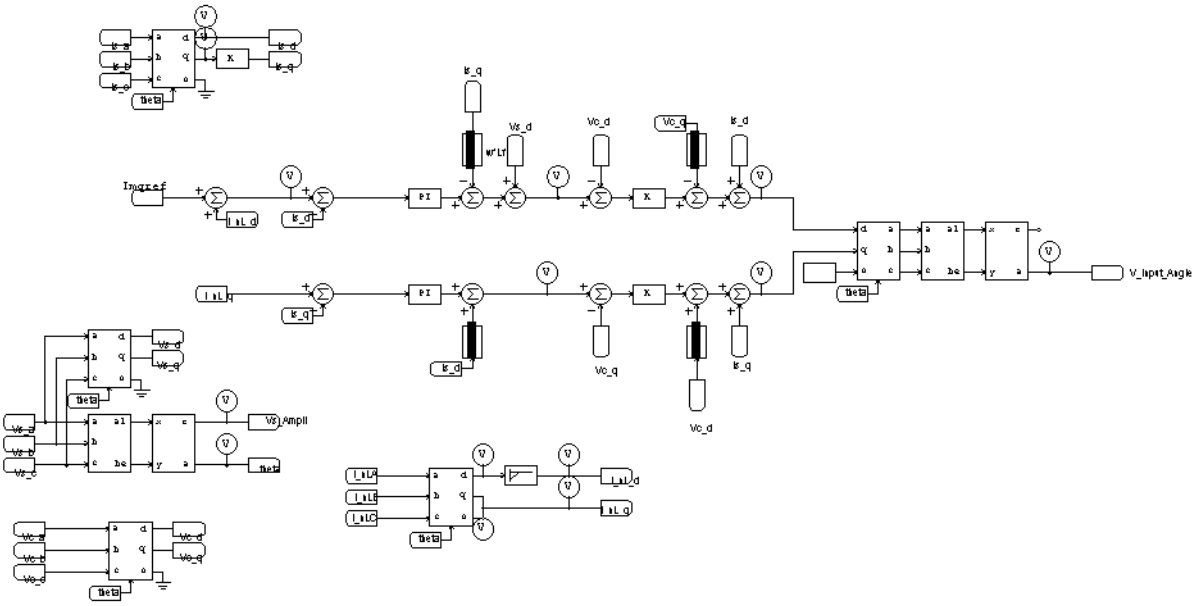

Figure B.3 Control system of the shunt active filter and 3-phase LC-filter

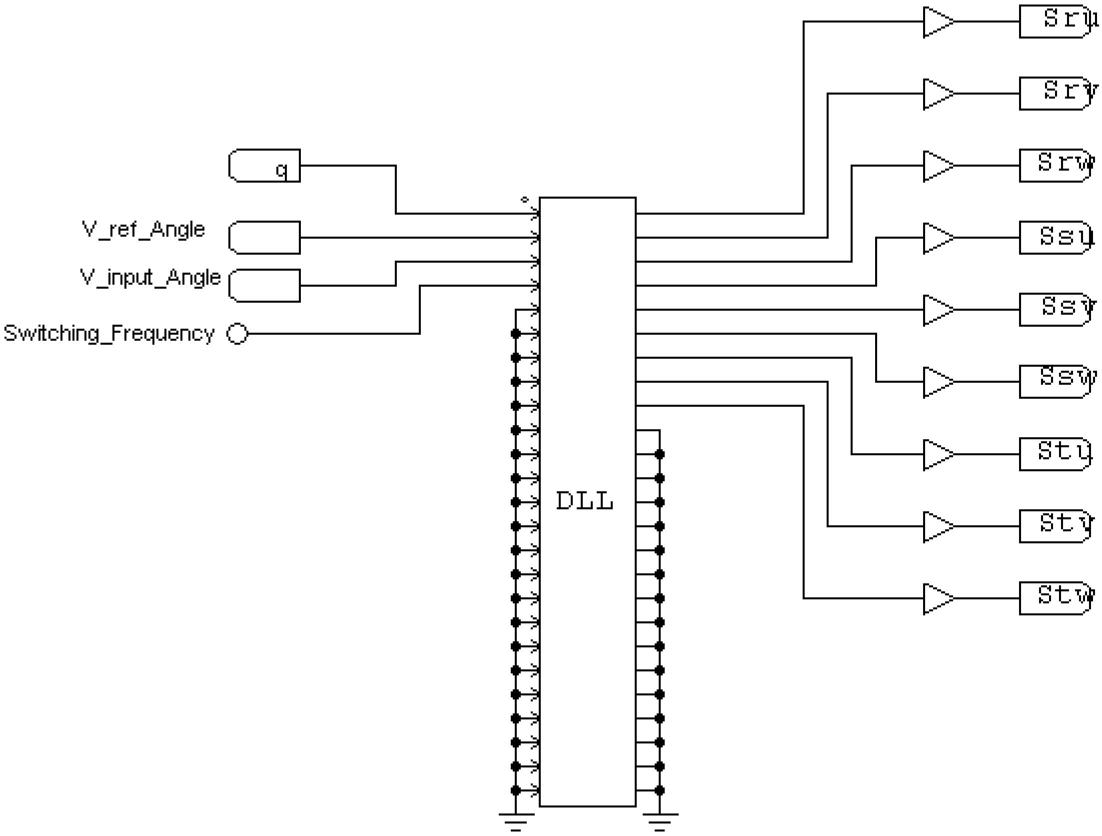


Figure B.4 Indirect space vector modulation

# Back-to-Back converter and its control system

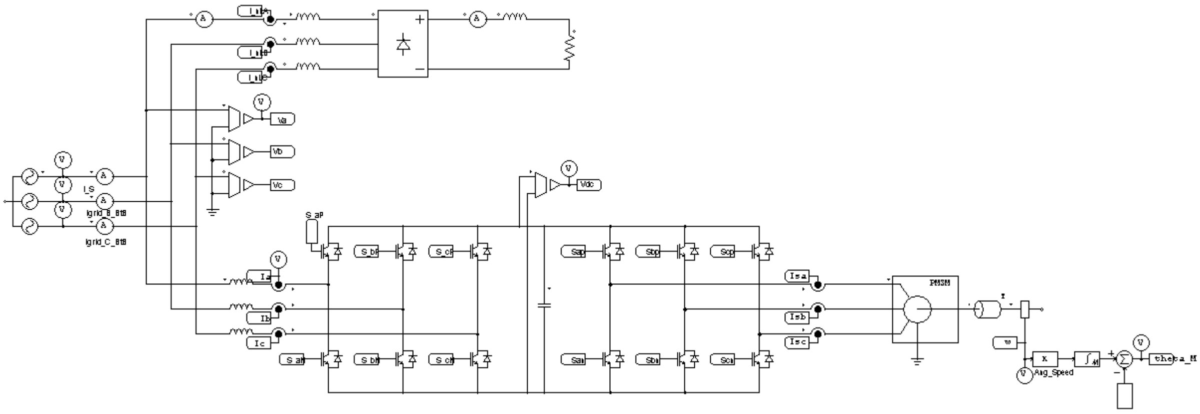

Figure B.5  Equivalent circuit of the Back-to-Back voltage source converter shunted to the nonlinear load

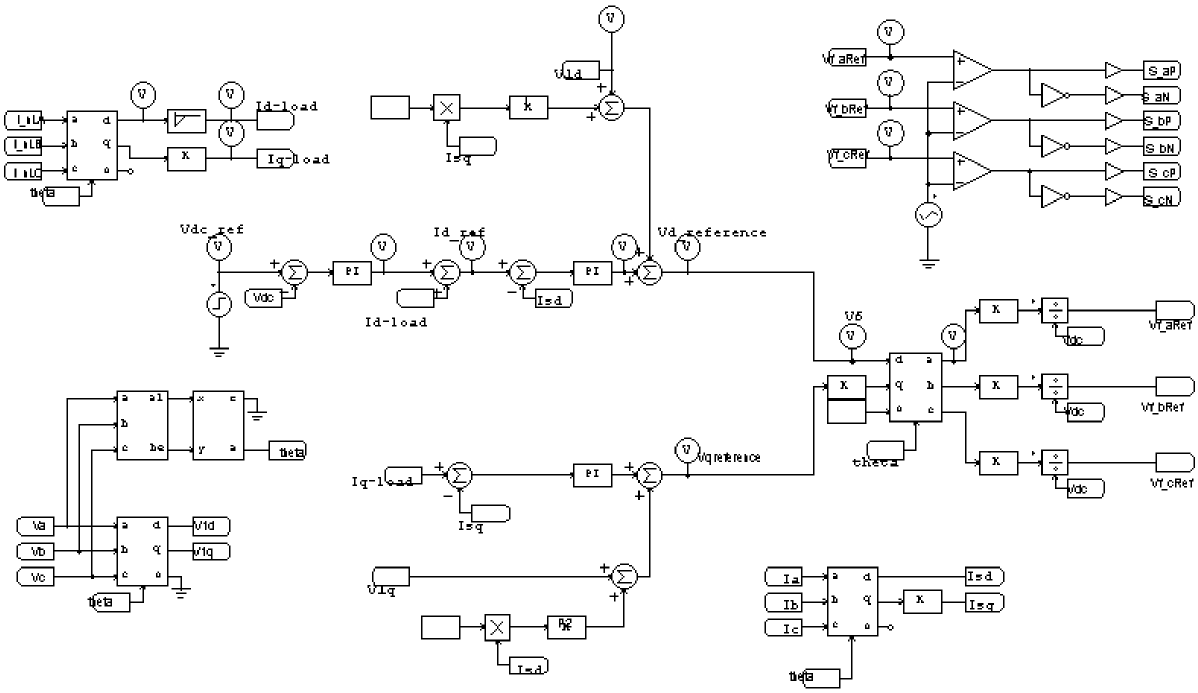


Figure B.6 Control system of the Active Front End filter

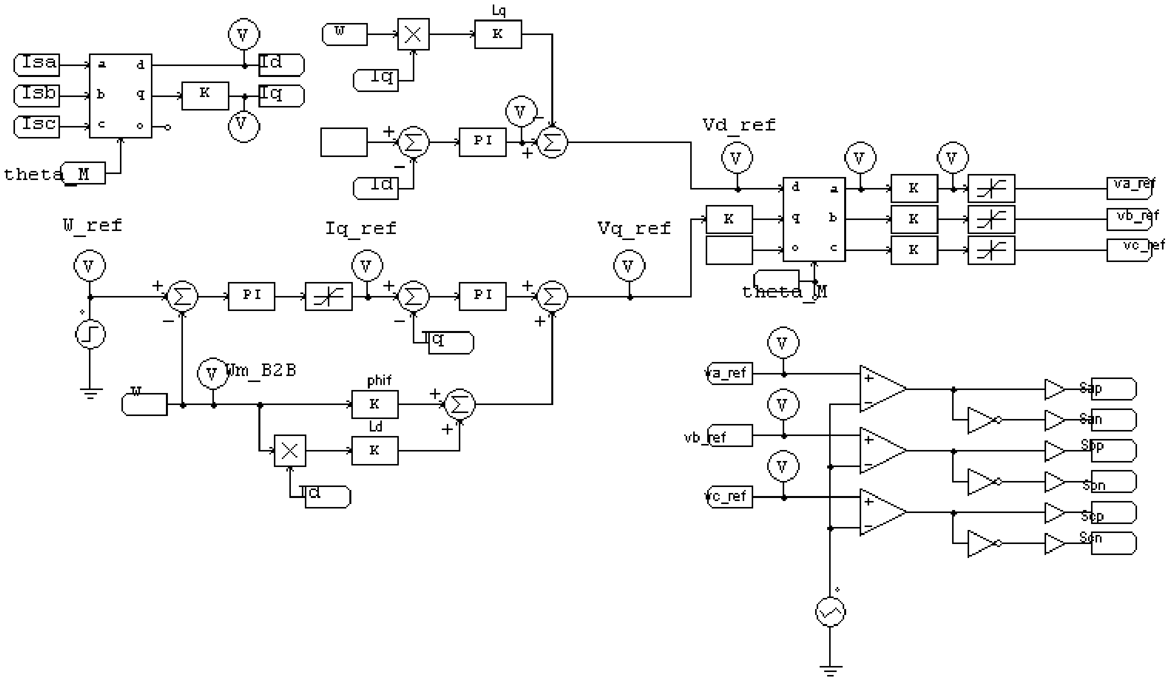


Figure B.7 Control system of the Permanent magnet synchronous machine